422297

Report 1741

DEPARTMENT OF THE NAVY

HYDROMECHANICS

o

AERODYNAMICS

o

STRUCTURAL MECHANICS

o

APPLIED MATHEMATICS

TESTS OF STIFFENED AND UNSTIFFENED MACHINED SPHERICAL SHELLS UNDER EXTERNAL HYDROSTATIC PRESSURE

by

Martin A. Krenzke and Thomas J. Kiernan

STRUCTURAL MECHANICS LABORATORY

RESEARCH AND DEVELOPMENT REPORT

August 1963

Report 1741

TESTS OF STIFFENED AND UNSTIFFENED MACHINED SPHERICAL SHELLS UNDER EXTERNAL HYDROSTATIC PRESSURE

by

Martin A. Krenzke and Thomas J. Kiernan

August 1963

Report 1741
S-R011 01 01

TABLE OF CONTENTS

LIST OF FIGURES

LIST OF TABLES

LIST OF TABLES (Cont'd)

ABSTRACT

Four series of structural models, consisting of 102 small machined spherical shells, were tested to study the effect of unsupported shell length on both their elastic and inelastic buckling strength. The four series consisted of models representing complete spheres, clamped spherical segment models with included angles ranging from 5 to 300 deg, and stiffened hemispherical models. The collapse pressure of the complete spheres was adequately calculated using the empirical equation earlier developed at the Model Basin. Whereas previous experiments on spherical shells with clamped edges recorded in the literature show a complete lack of repeatability, the results of the present models follow a definite pattern. These tests demonstrate that the unsupported shell length must be relatively short to provide an increase in strength of a spherical segment over that of a complete sphere. They also demonstrate that a small clamped spherical segment may be weaker than a longer clamped segment. The experimental collapse strength of the stiffened shells was in no case as great as would be expected for a machined unstiffened shell of the same weight. Since these were rather exploratory tests, however, they do not demonstrate that effective stiffening systems cannot be developed.

INTRODUCTION

The problem of the collapse strength of spherical shells under uniform pressure has received considerable attention in recent years. This attention is due in part to the introduction of missiles and other spacecraft, and in part to the academic interest which the problem arouses.[1]

Despite considerable effort by various investigators, there are no adequate design procedures for spherical shells.[2] This is particularly true for naval applications where relatively thick, deep spherical shells are involved. The theoretical work carried out thus far is of little value to the naval designer since the major effort has been directed toward the elastic buckling of shallow thin caps. This orientation in theoretical effort is due chiefly to the aeronautical application of this type of shell structure. However, it often appears that work in this area is also promoted by mathematical exploration of a problem somewhat more simple than that of a deep or complete sphere.[2] Experimental investigations have been considerably more limited than theoretical investigations. The limited experimental studies have normally involved shells much thinner than those of interest to the naval designer, and lack of sufficient knowledge of the initial imperfections present in the test specimens makes it impossible to obtain useful design guidance from the test results.

During the past two years, the David Taylor Model Basin has been actively engaged in developing the necessary background for the design of

---

1 References are listed on page 63.

spherical shells for use in underwater vehicles. Since recent emphasis has been placed on deep-depth applications such as TRIESTE, the strength of relatively thick as well as thin spherical shells is being investigated. A limited amount of theoretical work is being conducted, but the program is primarily experimental. Test specimens are being machined as well as manufactured according to feasible large-scale fabrication procedures. The effects of initial imperfections, residual stresses, boundary conditions, stiffening systems, and penetrations on elastic and inelastic behavior and collapse strength are being studied.

This report summarizes the test results of four series of small machined spherical models. These tests, which were conducted under the Fundamental Research Program (S-R011 01 01, Task 0401) and included 102 models, were designed to study the effect of unsupported shell length on elastic and inelastic collapse strength of initially near-perfect spherical shells. The current heavy workload of high-priority projects precludes conducting a complete analysis of the test results at this time. However, publication of this preliminary analysis appears warranted in view of the apparent lack of adequate experimental data in the literature on the buckling strength of spherical shells. The general effects of stiffening systems and initial departures from sphericity on collapse strength are discussed on the basis of this preliminary analysis.

HISTORICAL BACKGROUND

COMPLETE SPHERES

Timoshenko[3] summarized the classical small-defection theory for the elastic buckling of a complete sphere as first developed by Zoelly in 1915. In this analysis it is assumed that buckling will occur at that pressure which permits an equilibrium shape minutely removed from the perfectly spherical deflected shape. The expression for this classical buckling pressure p_1 may be given as

$$p_1 = \frac{2E\left(\frac{h}{R}\right)^2}{\sqrt{3(1-\nu^2)}} \qquad [1]$$

where E is Young's modulus,

h is the shell thickness,

R is the radius to the midsurface of the shell, and

ν is Poisson's ratio.

Unfortunately, the very limited data available prior to the current Model Basin program do not support the linear theory; elastic-buckling loads of roughly one-fourth those predicted by Equation [1] were observed in earlier tests recorded in the literature.[2,4]

Various investigators have attempted to explain this discrepancy by introducing nonlinear shell equations. Von Kármán and Tsien[5] initially introduced the nonlinear equations and the associated postbuckling configurations. They determined the minimum load required to keep an elastic shell in the postbuckle position of finite deformation and offered

this minimum value as the "lower" buckling load which could be expected in an ordinary experiment. Friedrichs[6] demonstrated that Von Kármán and Tsien erred in placing certain restrictions on deformations. However, when Friedrichs removed the restrictions on deformations and introduced a "boundary layer" concept, he was unable to obtain an equilibrium load in the postbuckle shape. Following Friedrich's work, Tsien[7] found that by introducing a new buckling concept, commonly referred to as the "energy criterion of jump," he could calculate postbuckling equilibrium loads.* This energy criterion assumes that:

1. the energy level must be the same before and after buckling, and

2. the geometric restraints of the loading device must be satisfied.

Although the theoretical predictions of Tsien are in fairly good agreement with the early test results, there is widespread belief that his minimum theoretical pressures have no true significance. For instance, Tsien's theory predicts buckling pressure to be a function of the size of the test chamber; collapse is predicted to occur at a lower pressure in a large test tank than in a small test tank, where the tank pressure falls off appreciably during buckling. In practice, however, no difference in buckling pressure due to the size or energy of the system has been observed.

Recently, Thompson[9] has determined both theoretically and experimentally that stable postbuckle states do exist for complete, "near-perfect"

* Unaware of Tsien's work due to the restricted exchange of scientific information during World War II, Yoshimina and Uemura of the University of Tokyo later developed a similar energy criterion.[8]

spherical shells. His minimum pressure of the postbuckle path, obtained theoretically by introducing a four-degree-of-freedom analysis, was found to be 0.24 times the classical pressure. Furthermore, Thompson also found that this "minimum pressure" had no relationship with the experimental buckling pressure.

The test specimens used in the earlier tests,[2,4] the results of which have been frequently compared to the theoretical buckling pressure for initially perfect spheres, were formed from flat plates. Thus, although little data are available, it can be assumed that these early specimens had significant departures from sphericity, variations in thickness, and residual stresses. Those specimens which were not complete spheres also had adverse boundary conditions. Until very recently,[9,10] however, no attempt has been made to theoretically evaluate these effects on the collapse strength of deep or complete spheres.

To clarify this rather large discrepancy between the classical buckling pressure and the existing experimental data, the Model Basin recently completed tests of two series of machined spherical shells[11,12] which more closely fulfilled the assumptions of linear theory than accomplished by the specimens tested in the earlier experiments. These tests demonstrated the effects of initial departures from sphericity, together with the normally less serious effects of variations in thickness, residual stresses, and adverse boundary conditions. The collapse strength of these machined shells was about two to four times greater than the collapse strength of the

shells formed from flat plate.[2,4] By achieving a maximum 0.9 ratio of experimental collapse pressure to the collapse pressure obtained from classical theory these tests lend considerable support to the validity of the small-deflection theory for initially perfect complete spheres. Based on these recent test results, an empirical design equation for machined spheres was suggested which predicts collapse to occur at about 0.7 times the classical pressure. For a Poisson's ratio of 0.3, this empirical equation for the elastic buckling pressure p_3 of near-perfect spheres may be expressed as

$$p_3 = 0.84\, E \left(\frac{h}{R_o}\right)^2 \qquad [2]$$

where the use of the outer radius R_o is dictated by simple load equilibrium.

Since the recent tests show that the discrepancy between the early experiments and the classical small-deflection theory can be attributed to the failure of the specimens to fulfill the rigid theoretical assumptions, it appears particularly worthwhile to investigate the effects of initial departures from sphericity on the elastic buckling strength of complete spheres. Until very recently, no theoretical or experimental work had been done in this area. However, Thompson[9] has recently conducted an "elementary study" of the theoretical behavior of a complete sphere with an initial departure from sphericity. Based on a middle surface imperfection of assumed shape and amplitude, he solved the nonlinear equations

for the maximum buckling pressure. This type of theoretical approach shows promise of producing the first valid theoretical analysis for practical spheres and appears worthy of further investigation. Tests have recently been conducted at the Model Basin to study the experimental buckling pressure of machined shells with known local "flat spots."[13] The collapse pressures of these "flat spot" specimens were adequately calculated using a semi-empirical equation developed on the basis of the results presented in this report.

Bijlaard,[14] Gerard,[15] and Lunchick[16] have developed solutions for the inelastic buckling of complete spheres. Each followed the same basic approach of applying a plasticity reduction factor to the classical linear theory. Except for the use of different expressions for Poisson's ratio in the plastic range, their solutions are identical. For a Poisson's ratio of 0.3 in the elastic region, Gerard's expression becomes

$$p_G = 1.154 \sqrt{\frac{E_s E_t}{(1-\nu_p^2)}} \left(\frac{h}{R}\right)^2 \qquad [3]$$

where E_s is the secant modulus,

E_t is the tangent modulus, and

ν_p is Poisson's ratio in the plastic range.

Thus, if it is assumed that Poisson's ratio in the plastic range remains at 0.3, Gerard's expression becomes

$$p_{G'} = 1.21 \sqrt{E_s E_t} \left(\frac{h}{R}\right)^2 \qquad [4]$$

Tests of machined aluminum spherical shells with ideal boundaries which collapsed at stress levels above the elastic limit of the material are also presented in Reference 11. For each model tested, the plastic buckling theories of References 14, 15, and 16 gave collapse pressures higher than the corresponding experimental collapse pressures. The collapse strength of those models which failed at stress levels above the proportional limit were accurately calculated, however, using an empirical formula based on the observed collapse strength of the elastic models (as estimated by Equation [2]) and a plasticity reduction factor similar to that developed in existing theory. This empirical formula for the inelastic collapse pressure of near-perfect spheres may be expressed as

$$p_E = 0.84 \sqrt{E_s E_t} \left(\frac{h}{R_o}\right)^2 \qquad [5]$$

The secant and tangent modulus used in Equations [3], [4], and [5] are derived from typical stress-strain curves of the material obtained from tests of simple compression specimens. In Equations [3] and [4] it is assumed, on the basis of thin shell theory, that the stress σ_1 may be calculated by

$$\sigma_1 = \frac{pR}{2h} \qquad [6]$$

In Equation [5], the average stress which satisfies equilibrium conditions for all thicknesses, σ_{avg}, is used and may be calculated by

$$\sigma_{avg} = \frac{pR_o^2}{2Rh} \qquad [7]$$

In many cases the presence of residual stresses lowers the collapse strength of spherical shells.[17] This is particularly true for those shells whose theoretical elastic collapse strength is only slightly greater than their inelastic collapse strength. Specifically, residual stresses normally cause a lowering of the proportional limit of the material and an associated falling off of the secant and tangent modulus. Formulas [3], [4], and [5] show that by reducing the secant and tangent modulus the collapse strength is reduced for such shells. Although it can be stated qualitatively that residual stresses have a detrimental effect on many spherical shells, there is no theory which may be used to quantitatively evaluate this effect. Furthermore, it is unlikely that a completely theoretical approach to this problem will be satisfactory since the residual stresses will probably often be present in some random, unpredictable pattern.

No significant work has been accomplished on the effects of penetrations and adverse boundary conditions on the collapse strength of spherical shells. A method has been developed at the Model Basin for designing penetrations and cylinder-hemisphere junctures for no rotation and for a radial deflection equal to that of all other parts of the spherical shell.[18] Thus, the effects of penetrations and boundary conditions on collapse pressure can be eliminated for ideal cases. For example, the membrane boundary cylinders for hemispherical shells,[11,12,19,20] the

reinforcement for axisymmetric penetrations in spherical shells,[19,20] and the reinforcement for viewing ports in spherical hulls for oceanographic research[21] have successfully been designed in this manner.

Since stability considerations control the design of spherical shells required to resist hydrostatic pressure on the convex side, it is worth investigating the possibility of increasing the structural efficiency of these shells by introducing stiffening systems. Unfortunately, no theory is available for the buckling strength of stiffened spherical shells. However, considerable theoretical work has been done on the buckling of clamped spherical segments, and this work is indirectly associated with the local buckling of stiffened spherical shells. Experimental data on the strength of stiffened spherical shells are lacking. Kloppel and Jungbluth[4] were unsuccessful in their attempts to improve structural efficiency by stiffening spherical shells. However, the Model Basin has recently conducted tests which indicate that some advantages may possibly be gained by stiffening welded HY-80 steel spherical shells.[17]

SPHERICAL SEGMENTS WITH CLAMPED BOUNDARIES

The perfect complete sphere deforms uniformly under pressure, but the spherical segment with clamped boundaries distorts axisymmetrically at the initiation of the uniform pressure loading. Thus, nonlinear equations must be introduced in order to determine the elastic behavior of clamped spherical segments.

The nonlinear theory for the elastic buckling strength of near-perfect shallow spherical segments with clamped edges under external hydrostatic pressure was first investigated by Feodosiev[22] in 1946. Since that time, the problem has received considerable attention. The more recent work of Budiansky,[23] Weinitschke,[24] and Thurston[25] are particularly noteworthy since they are in good agreement with each other throughout the range of shallow spherical segments.* In contrast, the results of the earlier studies based on nonlinear equations conducted by Feodosiev,[22] Kaplan and Fung,[26] and several other investigators[27,28,29] are generally in disagreement with each other.

Although Budiansky,[23] Weinitschke,[24] and Thurston[25] have independently developed solutions for the elastic axisymmetric buckling of shallow spherical segments which agree well with each other, there is generally very poor agreement between their theoretical predictions and existing experiments.[4,7,26,30] This disagreement is normally attributed to the presence of initial imperfections in the test specimens and to the influence of the nonsymmetric buckling mode, neither of which are considered in these theories.[23,24,25] The effect of initial imperfections in the elastic axisymmetric buckling of shallow segments has been studied by Chen[31] and Budiansky.[23] Although both investigators have shown that the presence of initial imperfections lowers the theoretical elastic

* A spherical segment is considered to be shallow when the ratio of its height to its base radius is less than one-eighth.[26]

axisymmetric buckling pressure, the calculated reduction in buckling pressure based on measured initial imperfection is not nearly enough to produce even fair agreement with the experimental data.[23] Weinitschke[32] recently presented a theory on the nonsymmetric buckling of spherical segments at an NASA Symposium on Instability of Shell Structures. At this symposium, Fung and Thurston and also Budiansky and Huang indicated that they were working on the same problem. Although Weinitschke's theory is in fairly good agreement with existing experiments, it differs considerably from the independent results which the other investigators are currently obtaining.

Very little work has been conducted on the inelastic strength of clamped spherical segments. By use of the theories of limit analysis, Hodge[33] derived the upper and lower bounds on the plastic collapse load of a spherical segment. Roth[34] studied the buckling of a spherical segment of an elastic perfectly plastic material. The inelastic buckling strength of a clamped spherical segment of strain-hardening material has not been studied. No experimental data on the inelastic buckling strength of clamped spherical segments can be found in the literature.

DESCRIPTION OF MODELS

The four series of models were designed to study the effect of unsupported shell length on collapse strength and consisted of the following:

1. Series S consisted of four models representing complete spheres.

2. Series SS consisted of 73 clamped spherical segment models with included angles ranging from 5 to 120 deg.

3. Series DSS consisted of eight 300-deg spherical segments with clamped edges.

4. Series SSS consisted of 17 stiffened hemispherical shells.

Nine models in Series SSS had circumferential stiffeners only, four had meridional stiffeners only, and four had both circumferential and meridional stiffeners.

Each series was designed to study both the elastic and inelastic buckling strength of spherical shells. Thus, the ratios of shell thickness to radius were selected to study relatively stable as well as unstable configurations. Unfortunately, the thinnest shells in Series S and Series DSS possessed ratios of shell thickness to radius which were slightly too great to ensure completely elastic failures.

All models in each series were machined from 7075-T6 aluminum bar stock with a nominal yield strength of 80,000 psi. Young's modulus E for the material, as determined by optical strain-gage measurements, was 10.8×10^6 psi. A Poisson's ratio ν of 0.3 in the elastic range was assumed. Tables 1-5 give the model dimensions for each series, and Figure 1 shows representative ratios of $\left[E_s E_t\right]^{1/2}$ to E as a function of uniaxial compressive stress for the material used in each model. The thickness used in all strength calculations is listed as measured wall thickness in these tables. Variations in measured thickness are also shown.

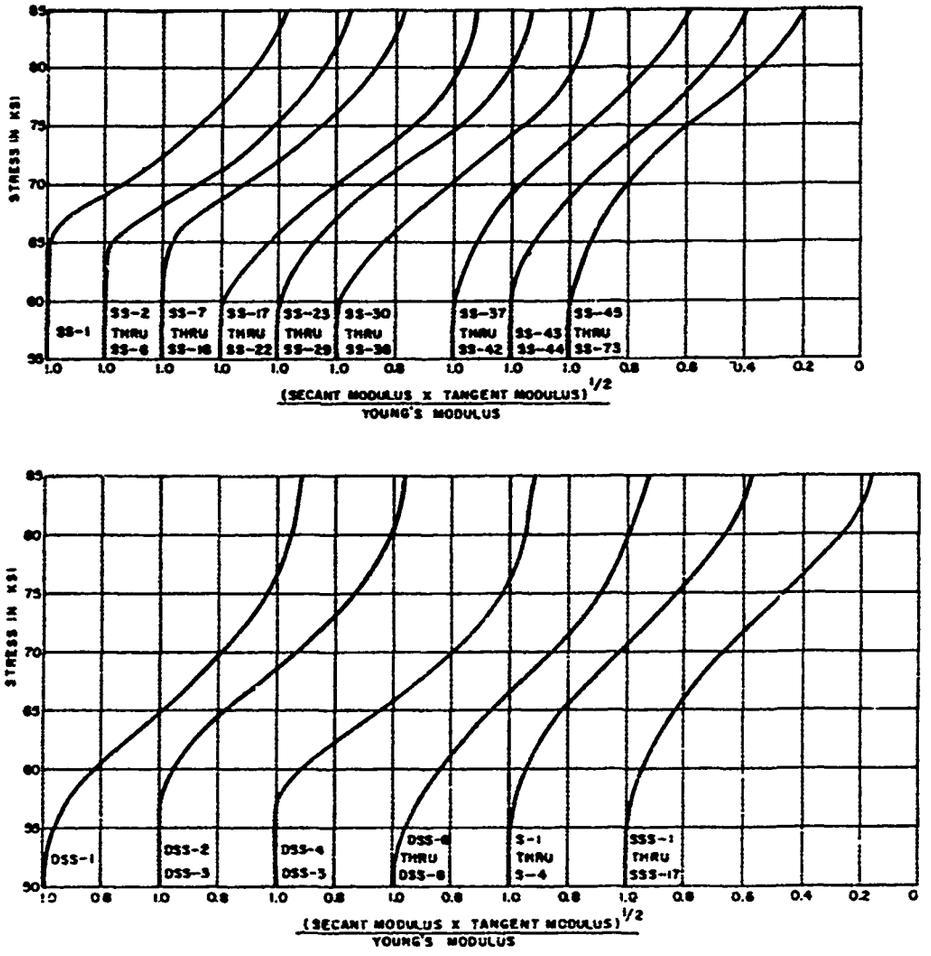

Figure 1 - Representative Material Characteristics

SERIES S

Series S consisted of four complete machined spheres, each having a 60-deg "hatch opening" required to permit machining of the inside contour. The "hatch covers," which were inserted into the opening, and the area in the shells adjacent to the opening were machined 10-percent thicker

than the remaining portion of the spheres in an effort to minimize boundary effects while discouraging failure in the cover itself (see Table 1).

Each of the four complete sphere models was machined in an identical manner. After roughing operations, the final contours of both the inside and outside of the main body of the sphere were obtained by profiling. The hatch covers were obtained by sawcutting disks from profiled hemispherical shells of the desired thickness, glueing the disks to a mating adaptor placed in a lathe, and machining the edges of the disk to match the opening in the sphere.

The wall thickness of each model was measured at numerous locations by means of a Vidigage. Unfortunately, the initial departures from sphericity were not determined for the Series S models.

SERIES SS

Series SS consisted of 73 machined spherical segment models with clamped edges; see Table 2. These models had included angles ranging from 5 to 120 deg. The interior contours of Models SS-1 through SS-56 were machined by use of form tools. The interior contours of Models SS-57 through 73 were generated after erratic results were obtained from the very thin models machined by form tools. In generating the interior contour of these models (which had very low ratios of wall thickness to radius), a tool specially designed to accurately generate inside spherical surfaces was used.* The outside spherical contour of each model was

* This same tool was used successfully (see Reference 12) to attain near-perfect sphericity in hemispherical shells.

TABLE 1

Dimensions and Experimental Collapse Pressures, Series S Models

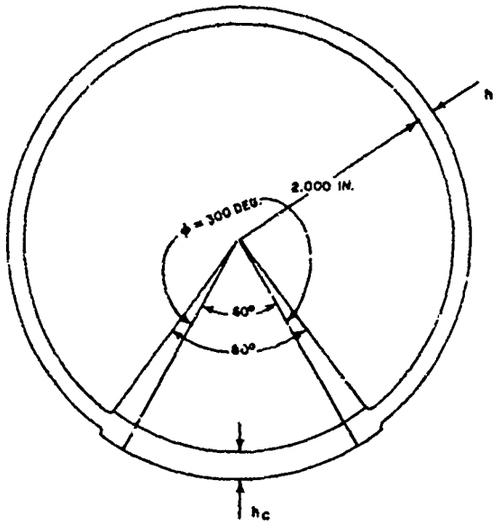

MODEL	Measured Wall Thickness h, in.	Measured Variation in h , in.	Cap Thickness h_c, in.	Experimental Collapse Pressure P_{exp} psi	Test Setup (see Figure 2)
S-1	0.193	+0.004 -0.001	0.227	14,300	A
S-2	0.121	+0.0010 -0.0015	0.141	8,500	A
S-3	0.0498	+0.0037 -0.0013	0.056	3,000	A
S-4	0.0260	±0.0018	0.029	1,500	A

TABLE 2

Dimensions and Experimental Collapse Pressures, Series SS Models

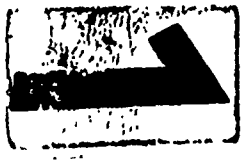

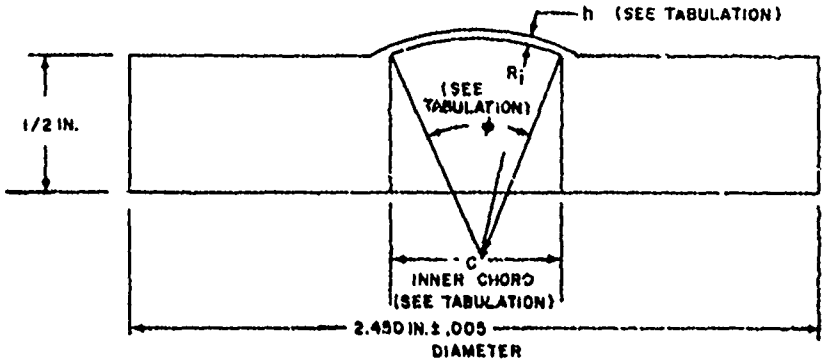

MODEL	Measured Wall Thickness h, in.	Measured Variation in h, in.	Inside Radius R_i, in.	Inner Chord C, in.	Included Angle ϕ deg	Experimental Collapse Pressure, p_{exp} psi	Test Setup (see Figure 2)
SS-1	0.0802	+0.0001 -0.0002	0.812	1.41	120	14,175	B
SS-2	0.0799	+0.0002 -0.0005	0.812	1.41	120	14,250	B
SS-3	0.0507	+0.0002 -0.0001	0.812	1.41	120	8,500	B
SS-4	0.0495	+0.0005 -0.0007	0.812	1.41	120	8,175	B
SS-5	0.0201	+0.0004 -0.0003	0.812	1.41	120	2,900	B
SS-6	0.0199	±0.0001	0.812	1.41	120	2,950	B
SS-7	0.0102	±0.0001	0.812	1.41	120	1,100	B
SS-8	0.0101	±0.0001	0.812	1.41	120	1,090	B
SS-9	0.0809	±0.0002	0.812	0.81	60	14,375	B
SS-10	0.0801	+0.0003 -0.0002	0.812	0.81	60	14,225	B
SS-11	0.0501	+0.0001 -0.0002	0.812	0.81	60	8,200	B
SS-12	0.0502	+0.0001 -0.0002	0.812	0.81	60	8,100	B
SS-13	0.0206	±0.0001	0.812	0.81	60	2,925	B
SS-14	0.0204	+0.0001 -0.0002	0.812	0.81	60	2,875	B
SS-15	0.0102	±0.0001	0.812	0.81	60	1,070	B
SS-16	0.0102	±0.0001	0.812	0.81	60	1,080	B
SS-17	0.08095	±0.0001	0.812	0.62	45	18,400	B
SS-18	0.0802	±0.0001	0.812	0.62	45	18,200	B
SS-19	0.0508	±0.0001	0.812	0.62	45	8,700	B
SS-20	0.0504	±0.0001	0.812	0.62	45	8,320	B
SS-21	0.0208	±0.0001	0.812	0.62	45	2,480	B

SS-18	0.0802	±0.0001	0.812	0.62	45	18,400	B
SS-19	0.0508	±0.0001	0.812	0.62	45	18,200	B
SS-20	0.0504	±0.0001	0.812	0.62	45	8,700	B
SS-21	0.0208	±0.0001	0.812	0.62	45	8,320	B
						2,480	B

SS-10	0.0901	+0.0003 -0.0002	0.812	0.81	60	14,225	B
SS-11	0.0501	+0.0001 -0.0002	0.812	0.81	60	8,200	B
SS-12	0.0502	+0.0001 -0.0002	0.812	0.81	60	8,100	B
SS-13	0.0206	±0.0001	0.812	0.81	60	2,925	B
SS-14	0.0204	+0.0001 -0.0002	0.812	0.81	60	2,875	B
SS-15	0.0102	±0.0001	0.812	0.81	60	1,070	B
SS-16	0.0102	±0.0001	0.812	0.81	60	1,080	B
SS-17	0.08095	±0.0001	0.812	0.62	45	18,400	B
SS-18	0.0802	±0.0001	0.812	0.62	45	18,200	B
SS-19	0.0508	±0.0001	0.812	0.62	45	8,700	B
SS-20	0.0504	±0.0001	0.812	0.62	45	8,320	B
SS-21	0.0208	±0.0001	0.812	0.62	45	2,480	B
SS-22	0.0207	±0.0001	0.812	0.62	45	2,545	B
SS-23	0.01045	±0.0001	0.812	0.62	45	1,060	B
SS-24	0.01035	±0.0001	0.812	0.62	45	1,055	B
SS-25	0.0057	±0.0001	0.812	0.62	45	355	B
SS-26	0.0051	±0.0001	0.812	0.62	45	290	B
SS-27	0.0554	±0.0001	0.812	0.42	30	18,550	B
SS-28	0.05515	±0.0001	0.812	0.42	30	18,375	B
SS-29	0.05055	±0.0001	0.812	0.42	30	16,320	B
SS-30	0.05025	±0.0001	0.812	0.42	30	15,930	B
SS-31	0.02035	±0.0001	0.812	0.42	30	2,725	B
SS-32	0.0204	±0.0001	0.812	0.42	30	2,700	B
SS-33	0.0106	±0.0001	0.812	0.42	30	735	B
SS-34	0.0103	±0.0001	0.812	0.42	30	685	B
SS-35	0.0049	±0.0001	0.812	0.42	30	270	B
SS-36	0.00465	±0.0001	0.812	0.42	30	195	B
SS-37	0.0803	±0.0001	2.00	0.70	20	14,375	B
SS-38	0.0798	±0.0001	2.00	0.70	20	14,250	B
SS-39	0.0450	±0.0001	2.00	0.70	20	4,350	B
SS-40	0.0439	±0.0001	2.00	0.70	20	4,150	B
SS-41	0.0225	±0.0001	1.95	0.70	20.6	945	D
SS-42	0.0230	±0.0	1.95	0.70	20.6	950	B
SS-43	0.0603	+0.0001 -0.0003	4.00	0.70	10	*	C
SS-44	0.0596	±0.0002	4.00	0.70	10	*	C
SS-45	0.0460	+0.0002 -0.0001	4.00	0.70	10	*	C
SS-46	0.0463	±0.0003	4.00	0.70	10	*	C
SS-47	0.0379	±0.0001	4.00	0.70	10	**	D
SS-48	0.0368	±0.0001	4.00	0.70	10	*	C
SS-49	0.0256	±0.0001	6.00	0.52	5	*	C
SS-50	0.0257	±0.0001	6.00	0.52	5	*	C
SS-51	0.0203	±0.0001	6.00	0.52	5	*	C
SS-52	0.0203	±0.0001	6.00	0.52	5	*	C
SS-53	0.0150	±0.0001	6.00	0.52	5	*	C
SS-54	0.0141	±0.0001	6.00	0.52	5	*	C
SS-55	0.0077	±0.0001	5.60	0.52	5.3	*	C
	0.0077	±0.0001	5.60	0.52	5.3	*	C
	0.0394	+0.0000 -0.0001	3.00	.86	16.5	2,050	D
	0.0346	+0.0001 -0.0000	3.00	.96	18.5	1,080	D
SS-57	0.0298	+0.0000 -0.0001	3.00	1.04	20.0	690	D
		+0.0000					

SS-37	0.0803	±0.0001	2.00	0.70	20	14,375	B
SS-38	0.0798	±0.0001	2.00	0.70	20	14,250	B
SS-39	0.0450	±0.0001	2.00	0.70	20	4,350	B
SS-40	0.0439	±0.0001	2.00	0.70	20	4,150	B
SS-41	0.0225	±0.0001	1.95	0.70	20.6	945	D
SS-42	0.0230	±0.0001	1.95	0.70	20.6	950	B
SS-43	0.0603	+0.0001 -0.0003	4.00	0.70	10	*	C
SS-44	0.0596	±0.0002	4.00	0.70	10	*	C
SS-45	0.0460	+0.0002 -0.0001	4.00	0.70	10	*	C
SS-46	0.0463	±0.0003	4.00	0.70	10	*	C
SS-47	0.0379	±0.0001	4.00	0.70	10	**	D
SS-48	0.0368	±0.0001	4.00	0.70	10	*	C
SS-49	0.0256	±0.0001	6.00	0.52	5	*	C
SS-50	0.0257	±0.0001	6.00	0.52	5	*	C
SS-51	0.0203	±0.0001	6.00	0.52	5	*	C
SS-52	0.0203	±0.0001	6.00	0.52	5	*	C
SS-53	0.0150	±0.0001	6.00	0.52	5	*	C
SS-54	0.0141	±0.0001	6.00	0.52	5	*	C
SS-55	0.0077	±0.0001	5.60	0.52	5.3	*	C
SS-56	0.0077	±0.0001	5.60	0.52	5.3	*	C
SS-57	0.0394	+0.0000 -0.0001	3.00	.86	16.5	2,050	D
SS-58	0.0346	+0.0001 -0.0000	3.00	.96	18.5	1,080	D
SS-59	0.0298	+0.0000 -0.0001	3.00	1.04	20.0	690	D
SS-60	0.0301	+0.0000 -0.0001	3.00	1.19	22.8	605	D
SS-61	0.0299	±0.0001	3.00	1.33	25.7	580	D
SS-62	0.0300	+0.0000 -0.0001	3.00	1.33	25.7	570	D
SS-63	0.0200	+0.0000 -0.0001	3.00	1.22	23.4	290	D
SS-64	0.0200	+0.0000 -0.0001	3.00	1.33	25.7	312	D
SS-65	0.0147	+0.0000 -0.0001	3.00	1.26	24.3	193	D
SS-66	0.0147	±0.0003	3.00	1.67	32.4	225	D
SS-67	0.0141	+0.0002 -0.0004	3.00	1.67	32.4	218	D
SS-68	0.0100	+0.0001 -0.0000	2.00	.97	28.1	226	D
SS-69	0.0096	±0.0002	2.00	1.31	38.1	213	D
SS-70	0.0107	±0.0001	2.00	1.57	46.0	257	D
SS-71	0.0105	±0.0001	2.00	1.82	54.0	249	D
SS-72	0.0105	±0.0001	2.00	2.00	60.0	246	D
SS-73	0.0104	+0.0000 -0.0001	2.00	1.20	35.0	245	D

* Model did not buckle; see Figure 6.
** Model did not buckle; see Figure 5.

obtained by supporting the inside contour by a mating mandrel and by generating the outside surface using a lathe with a ball-turning attachment. The edge of the spherical portion of each model was supported by a very heavy ring. The spherical shell and supporting ring of each model were machined as a unit.

Because each model was machined, a minimum of initial imperfections was anticipated. The wall thickness of each model was measured at numerous locations using a small support-ball and a dial gage calibrated in 0.00002 in. The total variation in measured wall thickness was normally less than 1 percent of the shell thickness. Deviations from perfect sphericity were not measured for Models SS-1 through SS-56. However, the variation in local inside radii was measured for the generated shells of Models SS-57 through SS-73 by pivoting a dial gage clamped to the special tool for generating inside spherical surfaces. These measurements indicated that the variation in local inside radii for each of these 17 shells after final machining was less than 0.0002 in. and normally less than 0.0001 in.

SERIES DSS

Series DSS consisted of eight machined 300-deg spherical shell models with clamped edges. Models DSS-1 through DSS-5 were machined by profiling both the interior and exterior spherical surfaces. The interior contours of Models DSS-6 through DSS-8 were generated using the new, specially designed tool which was also used for Models SS-57 through SS-73. The exterior contours of Models DSS-6 through DSS-8 were generated using a lathe with a ball-turning attachment. A heavy end ring

was machined integral with each 300-deg shell segment. In addition, a solid plug was placed inside the ring to provide additional rigidity at the edge of the spherical segments. These plugs had a nominal Class 4 fit with the mating end rings (see Table 3).

The shell thickness of Models DSS-1 through DSS-5 was measured by means of a Vidigage. The shell thickness of Models DSS-6 through DSS-8 was measured by using a small support-ball and a dial gage. No measurements of initial departures from sphericity were made on the Series DSS models.

SERIES SSS

Series SSS (see Tables 4 and 5) consisted of 17 externally stiffened machined hemispheres designed for an exploratory study of the effect of stiffening systems on the collapse strength of relatively unstable spherical shells. Models SSS-1 through SSS-9 had circumferential stiffeners only, Models SSS-10 through SSS-13 had meridional stiffeners only, and Models SSS-14 through SSS-17 had both circumferential and meridional stiffeners covering a portion of the hemispheres considered adequate to represent a complete sphere. The unstiffened portions of the hemispherical shells of Models SSS-14 through SSS-17 were of sufficient thickness to force failure to occur in the thinner region reinforced by the stiffeners (see Table 5).

The interior contours of each model were machined by use of a form tool. The exterior contours of Models SSS-1 through SSS-9 were machined by use of a lathe with a ball-turning attachment. The exterior

TABLE 3

Dimensions and Experimental Collapse Pressures, Series DSS Models

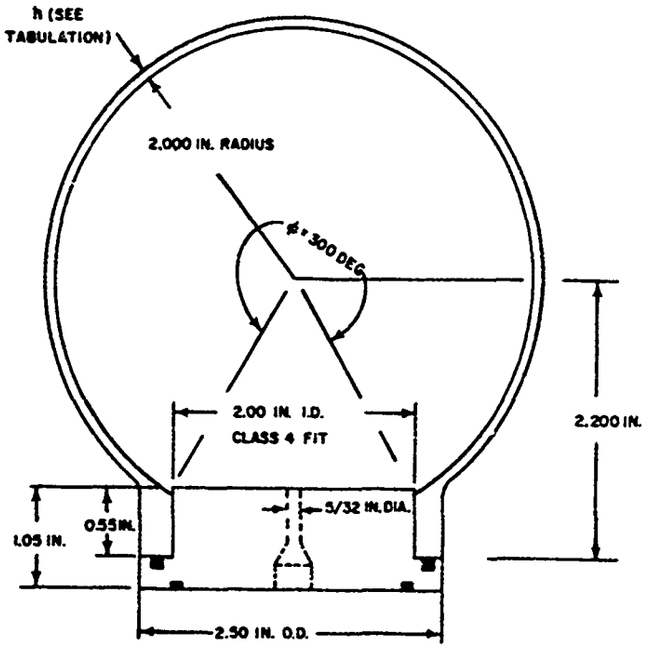

MODEL	Measured Wall Thickness h, in.	Measured Variation in h, in.	Experimental Collapse Pressure, Pexp psi	Test Setup (see Figure 2)
DSS-1	0.160	+0.003 -0.002	11,100	A
DSS-2	0.165	±0.005	11,375	A
DSS-3	0.0705	+0.0035 -0.0015	4,720	A
DSS-4	0.125	+0.005 -0.002	8,400	A
DSS-5	0.0505	+0.0015 -0.0005	2,800	A
DSS-6	0.0471	+0.0004 -0.0012	2,925	A
DSS-7	0.0224	+0.0006 -0.0006	1,200	A
DSS-8	0.0248	+0.0007 -0.0010	1,290	A

TABLE 4

Dimensions and Experimental Collapse Pressures, Series SSS Models SSS-1 through SSS-13

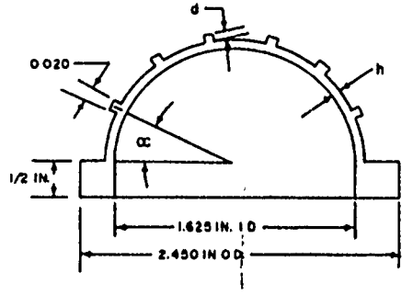

MODEL	Measured Wall Thickness, h, in.	Variation in Wall Thickness in.	Thickness of Stiffener, d, in.	Angle between Center of Stiffeners, α deg	Number of Stiffeners	Experimental Collapse Pressure, P_{exp} psi	Test Setup (see Figure 2)
SSS-1	0.0105	±0.0001	0.040	25.7	3	1100	B
SSS-2	0.0089	+0.0003 -0.0001	0.040	25.7	3	875	B
SSS-3	0.0074	±0.0002	0.030	13.85	6	700	B
SSS-4	0.0088	+0.0005 -0.0001	0.040	13.85	6	420	B

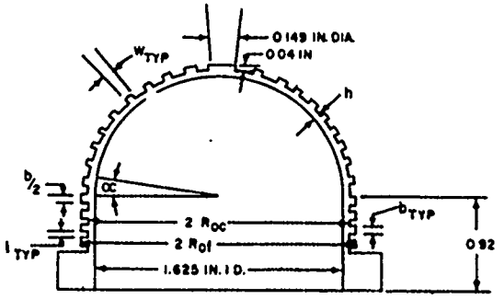

			Stiffeners on Hemisphere								
MODEL	Measured Wall Thickness, h, in.	Variation in Wall Thickness in.	Width of Stiffener, w, in.	Angle between Center of Stiffeners, α deg	Number of Stiffeners	b in.	$\frac{b}{2}$ in.	l in.	2 R_{OC} in.	2 R_{OI} in.	Experimental Collapse Pressure, P_{exp} psi
SSS-5*	0.0077	+0.0015 -0.0001	0.020	13.85	6	0.056	0.028	0.056	1.665	1.745	950
SSS-6*	0.0077	+0.0000 -0.0006	0.012	8.57	9	0.056	0.028	0.056	1.665	1.745	930
SSS-7*	0.0076	+0.0001 -0.0001	0.012	8.57	9	0.056	0.028	0.056	1.665	1.745	915
SSS-8*	0.0163	+0.0003 -0.0006	0.012	8.57	9	0.082	0.041	0.082	1.675	1.790	2740
		+0.0011									

SSS-6*	0.0077	+0.0000 -0.0006	0.012	8.57	9	0.056	0.028	0.056	1.665	1.745	930
SSS-7*	0.0076	+0.0001 -0.0001	0.012	8.57	9	0.056	0.028	0.056	1.665	1.745	915
SSS-8*	0.0163	+0.0003 -0.0006	0.012	8.57	9	0.082	0.041	0.082	1.675	1.790	2740
		+0.0011									

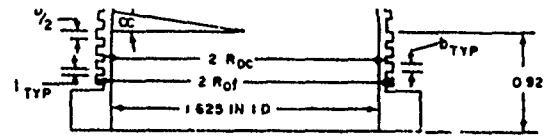

MODEL	Measured Wall Thickness, h, in.	Variation in Wall Thickness in.	Stiffeners on Hemisphere: Width of Stiffener, w, in.	Stiffeners on Hemisphere: Angle between Center of Stiffeners, α deg	Stiffeners on Hemisphere: Number of Stiffeners	b in.	b/2 in.	l in.	2 R_{oc} in.	2 R_{of} in.	Experimental Collapse Pressure, p_{exp} psi
SSS-5*	0.0077	+0.0015 -0.0001	0.020	13.85	6	0.056	0.028	0.056	1.665	1.745	950
SSS-6*	0.0077	+0.0000 -0.0006	0.012	8.57	9	0.056	0.028	0.056	1.665	1.745	930
SSS-7*	0.0076	+0.0001 -0.0001	0.012	8.57	9	0.056	0.028	0.056	1.665	1.745	915
SSS-8*	0.0163	+0.0003 -0.0006	0.012	8.57	9	0.082	0.041	0.082	1.675	1.790	2740
SSS-9*	0.0152	+0.0011 -0.0002	0.012	8.57	9	0.082	0.041	0.082	1.675	1.790	2390

* Test Setup B employed (see Figure 2).

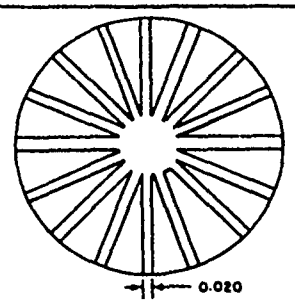

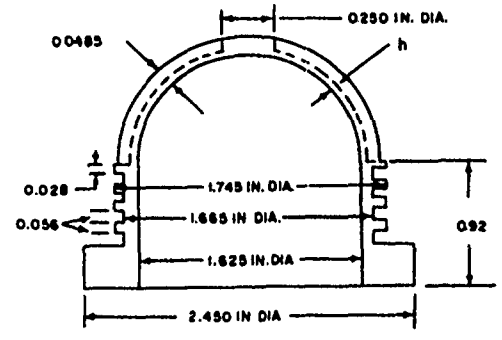

MODEL	Measured Wall Thickness, h, in.	Variation in Wall Thickness in.	Number of Stiffeners on Hemisphere	Experimental Collapse Pressure, p_{exp} psi	Test Setup (see Figure 2)
SSS-10	0.0046	+0.0013 -0.0001	8	265	B
SSS-11	0.0047	+0.0011 -0.0001	8	290	B
SSS-12	0.0062	+0.0014 -0.0002	8	435	B
SSS-13	0.0088	+0.0008 -0.0001	16	825	B

B	B
825	825
	16
+0.0008 -0.0001	+0.0008 -0.0001
0.0088	0.0088
SSS-13	SSS-13

TABLE 5

Dimensions and Experimental Collapse Pressures, Series SSS
Models SSS-14 and SSS-15

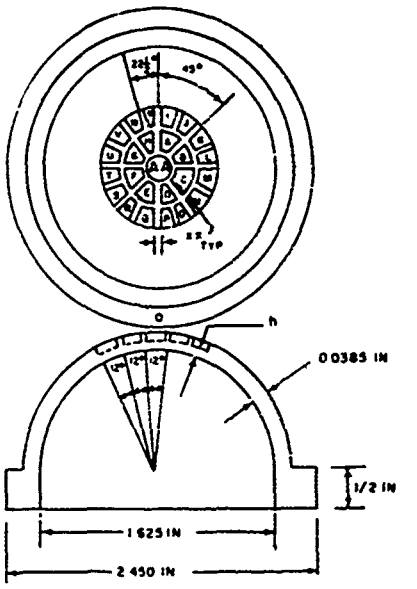

ELEMENT	Measured Thickness, in.			
	MODEL SSS-14*		MODEL SSS-15*	
	Maximum	Minimum	Maximum	Minimum
AA	0.0093	0.0083	0.0096	0.0092
A	0.0082	0.0079	0.0083	0.0078
B	0.0081	0.0075	0.0086	0.0082
C	0.0079	0.0076	0.0082	0.0076
D	0.0070	0.0066	0.0080	0.0077
E	0.0084	0.0070	0.0078	0.0076
F	0.0075	0.0070	0.0080	0.0074
G	0.0082	0.0073	0.0081	0.0076
H	0.0079	0.0077	0.0084	0.0076
I	0.0086	0.0084	0.0085	0.0079
J	0.0089	0.0086	0.0085	0.0080
K	0.0088	0.0086	0.0084	0.0079
L	0.0090	0.0089	0.0083	0.0079
M	0.0088	0.0085	0.0083	0.0079
N	0.0090	0.0089	0.0085	0.0080
O	0.0091	0.0088	0.0082	0.0077
P	0.0091	0.0089	0.0085	0.0079
Q	0.0088	0.0086	0.0081	0.0077
R	0.0086	0.0084	0.0084	0.0079
S	0.0085	0.0083	0.0084	0.0079
T	0.0087	0.0086	0.0087	0.0080
U	0.0085	0.0084	0.0085	0.0079
V	0.0088	0.0087	0.0086	0.0082
W	0.0084	0.0084	0.0082	0.0079
X	0.0088	0.0087	0.0084	0.0078
XX	0.014	0.010	0.014	0.011

* Experimental collapse pressures were 1325 psi for Model SSS-14 and 1345 ps. for Model SSS-15. The models buckled locally at lower pressures. Test Setup B was employed (see Figure 2).

TABLE 5 Continued

Dimensions and Experimental Collapse Pressures, Series SSS
Models SSS-16 and SSS-17

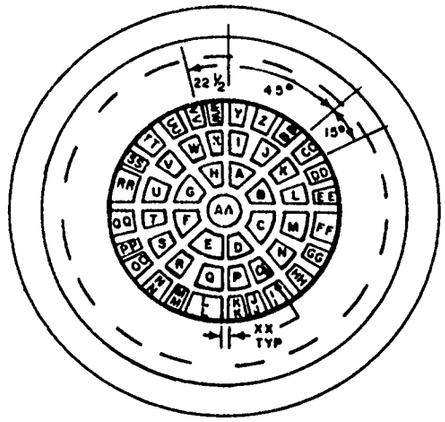

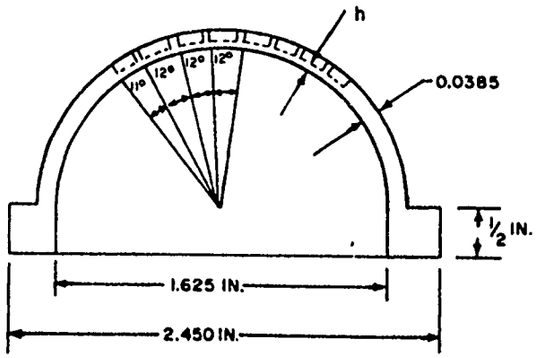

ELEMENT	Measured Thickness, in.			
	MODEL SSS-16**		MODEL SSS-17**	
	Maximum	Minimum	Maximum	Minimum
AA	0.0080	0.0065	0.0055	0.0053
A	0.0075	0.0071	0.0053	0.0051
B	0.0069	0.0067	0.0053	0.0051
C	0.0068	0.0066	0.0054	0.0052
D	0.0071	0.0068	0.0054	0.0052
E	0.0070	0.0065	0.0050	0.0048
F	0.0074	0.0072	0.0055	0.0053

F	0.0074	0.0072	0.0055	0.0053

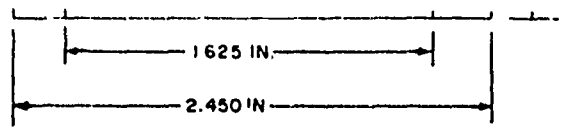

ELEMENT	Measured Thickness, in.			
	MODEL SSS-16**		MODEL SSS-17**	
	Maximum	Minimum	Maximum	Minimum
AA	0.0080	0.0065	0.0055	0.0053
A	0.0075	0.0071	0.0053	0.0051
B	0.0069	0.0067	0.0053	0.0051
C	0.0068	0.0066	0.0054	0.0052
D	0.0071	0.0068	0.0054	0.0052
E	0.0070	0.0065	0.0050	0.0048
F	0.0074	0.0072	0.0055	0.0053
G	0.0074	0.0073	0.0053	0.0051
H	0.0076	0.0071	0.0053	0.0051
I	0.0067	0.0066	0.0052	0.0049
J	0.0065	0.0064	0.0050	0.0047
K	0.0069	0.0067	0.0053	0.0049
L	0.0067	0.0065	0.0053	0.0051
M	0.0069	0.0067	0.0053	0.0049
N	0.0068	0.0066	0.0054	0.0052
O	0.0064	0.0063	0.0054	0.0052
P	0.0069	0.0067	0.0052	0.0050
Q	0.0068	0.0066	0.0053	0.0050
R	0.0067	0.0066	0.0050	0.0046
S	0.0065	0.0064	0.0050	0.0047
T	0.0068	0.0066	0.0051	0.0047
U	0.0066	0.0065	0.0051	0.0049
V	0.0065	0.0064	0.0050	0.0046
W	0.0067	0.0066	0.0049	0.0045
X	0.0066	0.0064	0.0050	0.0046
Y	0.0072	0.0070	0.0059	0.0057
Z	0.0076	0.0074	0.0062	0.0060
BB	0.0075	0.0074	0.0062	0.0059
CC	0.0074	0.0072	0.0062	0.0060
DD	0.0072	0.0071	0.0062	0.0060
EE	0.0070	0.0069	0.0062	0.0060
FF	0.0072	0.0071	0.0061	0.0059
GG	0.0074	0.0072	0.0059	0.0057
HH	0.0074	0.0073	0.0060	0.0057
II	0.0073	0.0070	0.0062	0.0059
JJ	0.0071	0.0069	0.0058	0.0056
KK	0.0068	0.0066	0.0059	0.0055
LL	0.0068	0.0066	0.0060	0.0058
MM	0.0070	0.0068	0.0064	0.0060
NN	0.0070	0.0069	0.0060	0.0058
OO	0.0072	0.0070	0.0060	0.0058
PP	0.0073	0.0071	0.0062	0.0060
QQ	0.0073	0.0071	0.0064	0.0062
RR	0.0073	0.0071	0.0063	0.0062
SS	0.0073	0.0071	0.0063	0.0061

XX	0.0073	0.0071	0.0063	0.0062

D	0.0071	0.0068	0.0054	0.0052
E	0.0070	0.0065	0.0050	0.0048
F	0.0074	0.0072	0.0055	0.0053
G	0.0074	0.0073	0.0053	0.0051
H	0.0076	0.0071	0.0053	0.0051
I	0.0067	0.0066	0.0052	0.0049
J	0.0065	0.0064	0.0050	0.0047
K	0.0069	0.0067	0.0053	0.0049
L	0.0067	0.0065	0.0053	0.0051
M	0.0069	0.0067	0.0053	0.0049
N	0.0068	0.0066	0.0054	0.0052
O	0.0064	0.0063	0.0054	0.0052
P	0.0069	0.0067	0.0052	0.0050
Q	0.0068	0.0066	0.0053	0.0050
R	0.0067	0.0066	0.0050	0.0046
S	0.0065	0.0064	0.0050	0.0047
T	0.0068	0.0066	0.0051	0.0047
U	0.0066	0.0065	0.0051	0.0049
V	0.0065	0.0064	0.0050	0.0046
W	0.0067	0.0066	0.0049	0.0045
X	0.0066	0.0064	0.0050	0.0046
Y	0.0072	0.0070	0.0059	0.0057
Z	0.0076	0.0074	0.0062	0.0060
BB	0.0075	0.0074	0.0062	0.0059
CC	0.0074	0.0072	0.0062	0.0060
DD	0.0072	0.0071	0.0062	0.0060
EE	0.0070	0.0069	0.0062	0.0060
FF	0.0072	0.0071	0.0061	0.0059
GG	0.0074	0.0072	0.0059	0.0057
HH	0.0074	0.0070	0.0060	0.0057
II	0.0073	0.0070	0.0062	0.0059
JJ	0.0071	0.0069	0.0058	0.0056
KK	0.0068	0.0066	0.0059	0.0055
LL	0.0068	0.0066	0.0060	0.0058
MM	0.0070	0.0068	0.0064	0.0060
NN	0.0070	0.0069	0.0060	0.0058
OO	0.0072	0.0070	0.0060	0.0058
PP	0.0073	0.0071	0.0062	0.0060
QQ	0.0073	0.0071	0.0064	0.0062
RR	0.0073	0.0071	0.0063	0.0062
SS	0.0073	0.0071	0.0063	0.0061
TT	0.0074	0.0071	0.0064	0.0062
UU	0.0073	0.0071	0.0066	0.0064
VV	0.0074	0.0072	0.0062	0.0059
WW	0.0073	0.0071	0.0061	0.0059
XX	0.014	0.010	0.014	0.010

** Experimental collapse pressures were 1125 psi for Model SSS-16 and 870 psi for Model SSS-17. The models buckled locally at lower pressures. Test Setup B was employed (see Figure 2).

contours of Models SSS-10 through SSS-17 were obtained by first turning the contour to the outside radius of the stiffeners and the thick-walled portions of the shell. Then the material between stiffeners was removed individually by indexing the model in relation to an electrode in an electric discharge machine. Thus, the stiffeners and shell formed an integral unit.

The wall thickness of each model was measured by using a small ball-support and a dial gage. The initial departures from sphericity were not measured in the Series SSS models.

TEST PROCEDURE

Each model was tested under external hydrostatic pressure. Schematic sketches of the pressure tanks and test setups are shown in Figure 2. Pressure was applied in increments and each new pressure level was held at least 1 min. The final pressure increment was normally less than 2 percent of the maximum pressure. Every effort was made to minimize any pressure surge when applying load.

SERIES S

Models S-1, S-2, S-3, and S-4 were tested in a 5-in.-diameter tank shown in Test Setup A of Figure 2. No strain data or change in internal volume measurements were recorded during the tests.

SERIES SS

Models SS-1 through SS-40 and Model SS-42 were tested in a 2-in.-diameter tank shown in Test Setup B of Figure 2. The models were

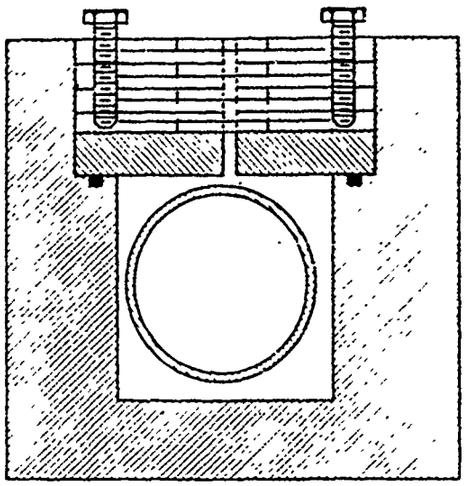

Figure 2a - Test Setup A

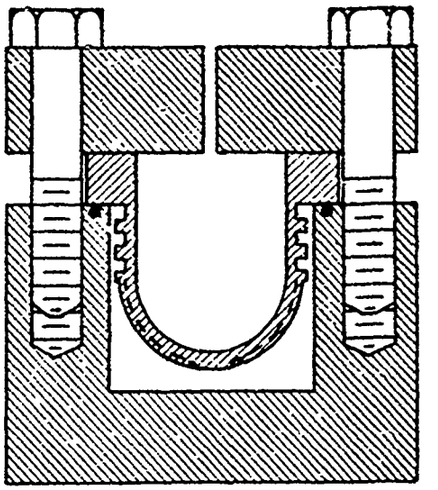

Figure 2b - Test Setup B

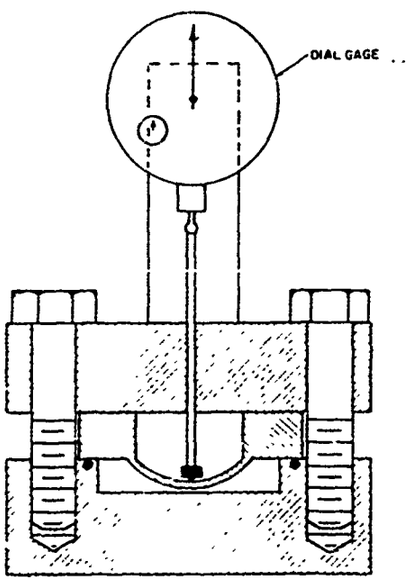

Figure 2c - Test Setup C

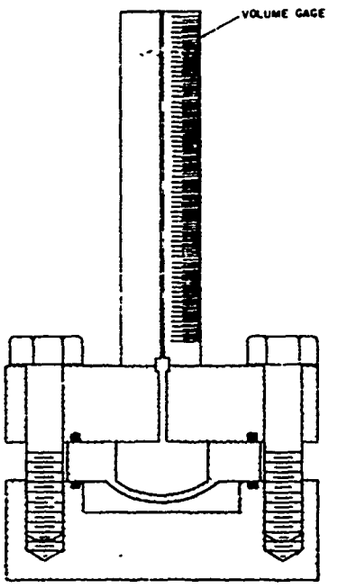

Figure 2d - Test Setup D

Figure 2 - Sketches of Models in Pressure Tanks

vented to the atmosphere. No strain d[illegible] or change in internal volume measurements were recorded during the tests. Models SS-43 through SS-46 and Models SS-48 through SS-56 were tested in a short, 2-in.-diameter tank shown in Test Setup C of Figure 2. No strain data were recorded during the tests. However, the center deflection of these models resulting from the applied hydrostatic load was recorded. Model SS-41, Model SS-47, and Models SS-57 through SS-73 were also tested in the short, 2-in.-diameter tank. However, the change in internal volume resulting from the applied load was recorded for these models rather than the center deflection. The test setup is shown in Figure 2d.

SERIES DSS

Models DSS-1 through DSS-8 were tested in the 5-in.-diameter tank shown in Test Setup A of Figure 2. No change in internal volume measurements was recorded. However, circumferential and meridional strains in Models DSS-4, DSS-5, and DSS-7 were recorded using foil-resistance strain gages. Gage locations are shown in Figure 3.

SERIES SSS

Models SSS-1 through SSS-17 were tested in the 2-in.-diameter tank shown in Test Setup B of Figure 2. No strain data or internal volume measurements were recorded during the tests. However, visual inspection of the inside contour of the model was conducted at all pressure increments prior to collapse for Models SSS-14 through SSS-17.

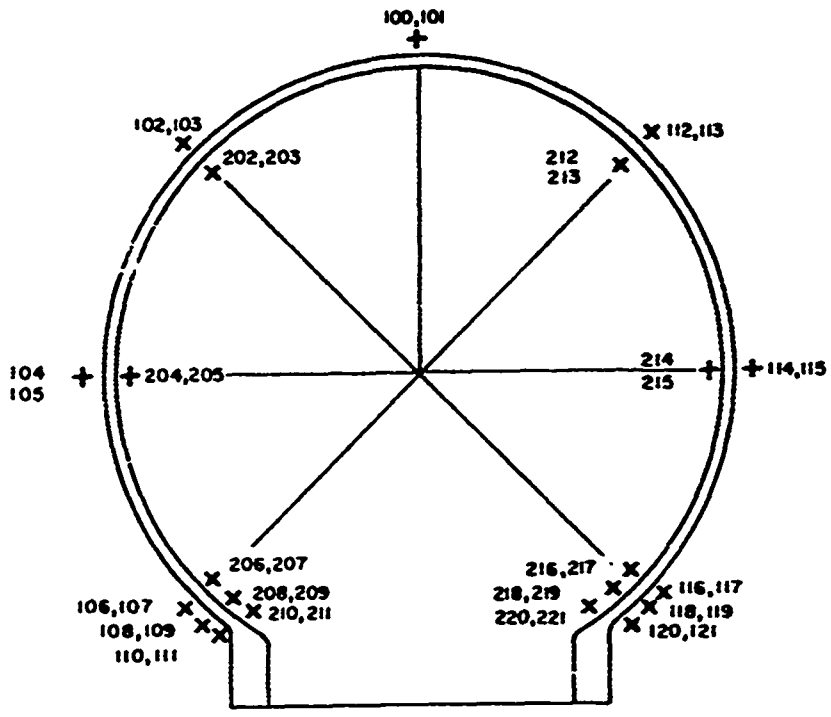

Figure 3 - Strain-Gage Locations for Series DSS, Models DSS-4, DSS-5, and DSS-7

TEST RESULTS

Models SS-43 through SS-56 were not collapsed or ruptured under external pressure. The collapse pressures for all other models are listed in Tables 1-5. Collapse pressure, defined as the maximum external pressure withstood by the respective model, was accompanied in each case by a large dropoff in tank pressure. Many of the models ruptured during collapse. Photographs of representative models after collapse are shown in Figure 4.

SERIES S

Each model in Series S ruptured during collapse (see Figure 4a). Failure of each model apparently initiated in the main body of the sphere.

Figure 4 - Samples of Collapsed Models

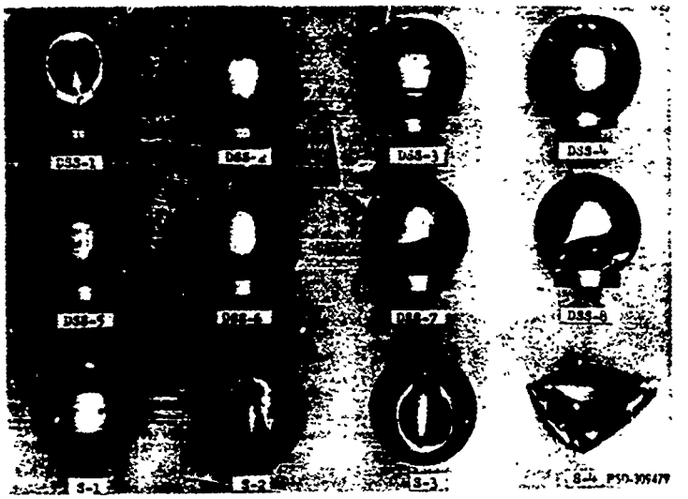

Figure 4a - Series S and Series DSS

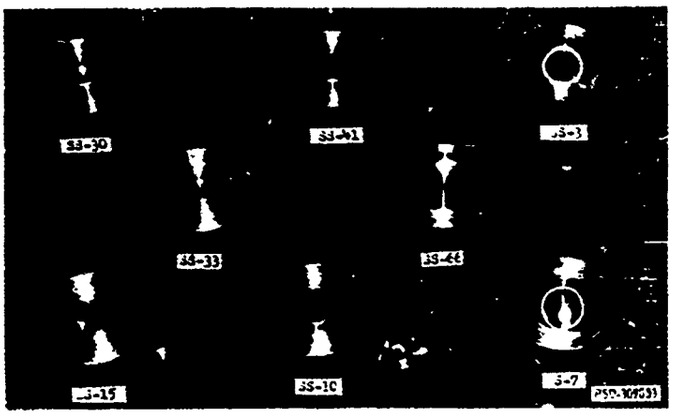

Figure 4b - Series SS

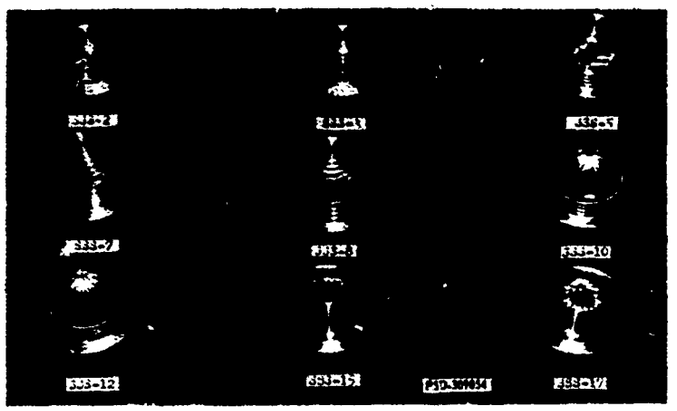

Figure 4c - Series SSS

Due to the relatively large size of the test tank, no falloff in tank pressure occurred prior to collapse of Series S Models.

SERIES SS

Models SS-1 through SS-42 and Models SS-57 through SS-73 each collapsed in a sudden, unmistakable manner. A slight falloff in tank pressure was observed prior to collapse of several of the more stable models. When this falloff in pressure was observed, the tank pressure was promptly raised to the proper level. Some of the models collapsed in a non-symmetric mode, and others apparently collapsed in a symmetric mode. The recorded changes in internal volume versus pressure for Model SS-41, Models SS-57 through SS-66, and Models SS-68 through SS-73 are presented in Figure 5.

Models SS-43 through SS-56 were not collapsed nor did they rupture under external pressure. Each model was subjected to pressures which caused the center deflection to be greater than the initial rise of the

Figure 5 - Pressure versus Relative Change in Internal Volume for Shallow Models of Series SS

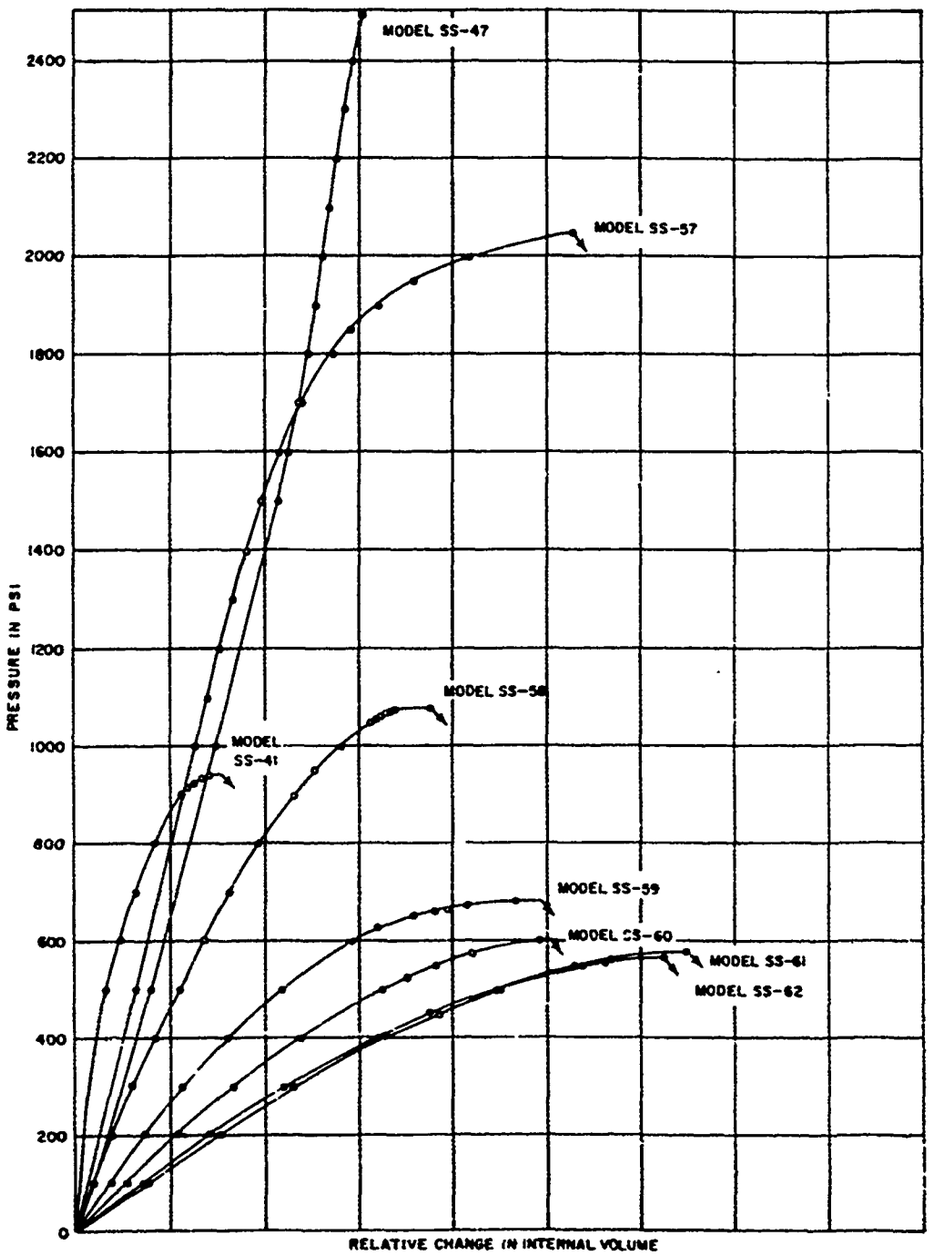

Figure - 5a

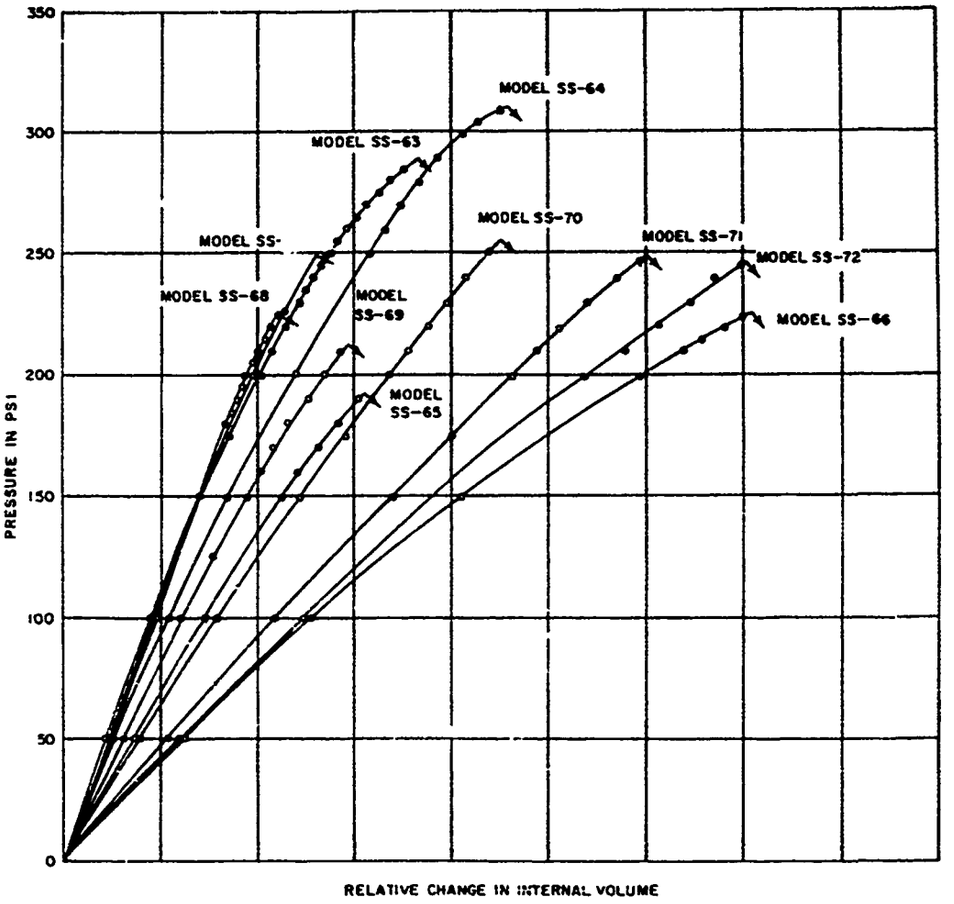

Figure - 5b

segment without buckling. The measured center deflection versus external pressure for each of these models except SS-47 is presented in Figure 6. The measured change in internal volume versus external pressure for Model SS-47 is shown in Figure 5.

SERIES DSS

Models DSS-1 through DSS-8 each ruptured during collapse (see Figure 4a). Failure of Models DSS-7 and DSS-8 initiated in the shell at

Figure 6 - Pressure versus Center Deflection for Shallow Models of Series SS

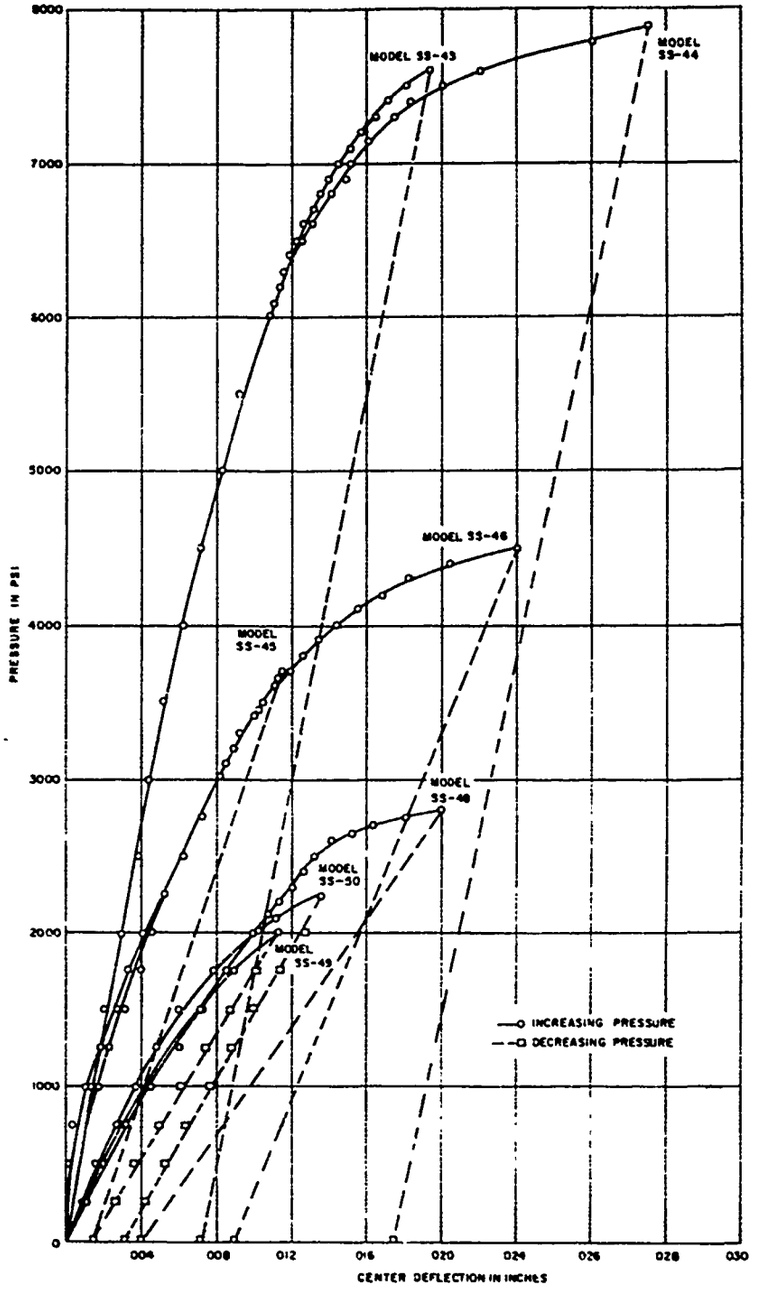

Figure - 6a

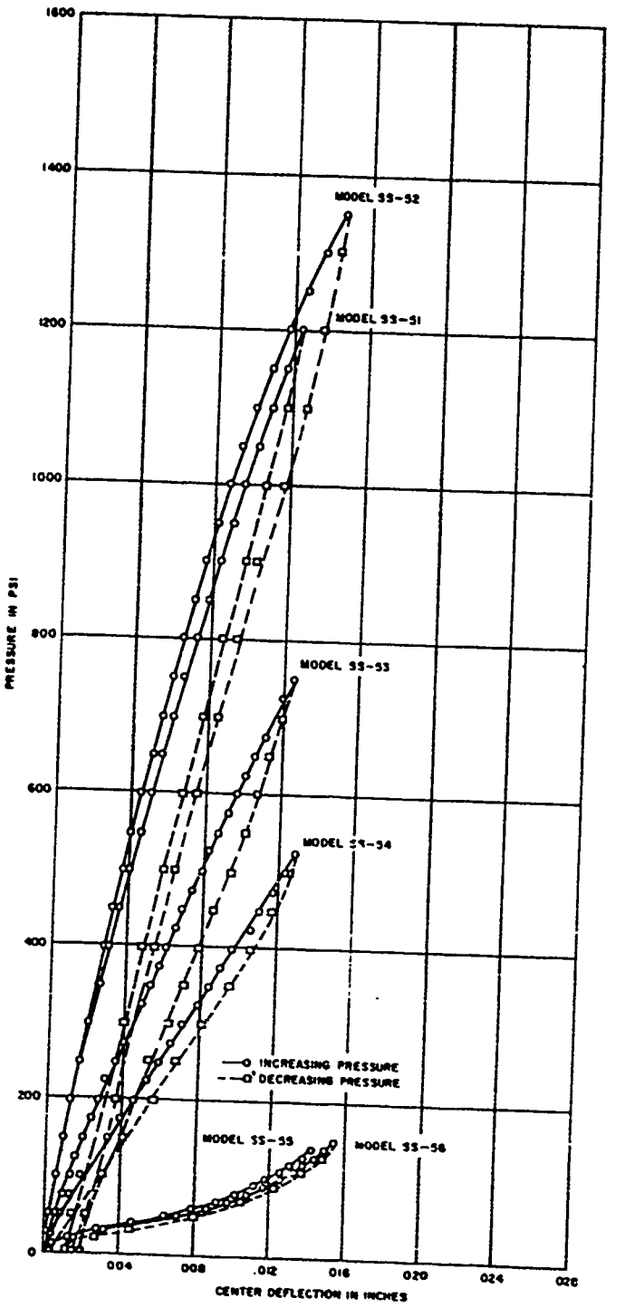
1600
1400
1200
1000
800
600
400
200
0
PRESSURE IN PSI
MODEL SS-52
MODEL SS-51
MODEL SS-53
MODEL SS-54
INCREASING PRESSURE
DECREASING PRESSURE
MODEL SS-55
MODEL SS-56
004
008
.012
016
020
024
028
CENTER DEFLECTION IN INCHES

Figure - 6b

the juncture with the heavy end ring. The other models failed in the shell in areas away from the end ring. Due to the relative size of the test tank, no falloff in tank pressure was observed prior to collapse of Series DSS models.

Measured elastic strain sensitivities, the initial slope of the pressure-strain plot, are presented for Models DSS-4, DSS-5, and DSS-7 in Figure 7. Typical plots of pressure versus strain are shown in Figure 8.

SERIES SSS

Models SSS-1 through SSS-13 failed in a very sudden manner. No drop in pressure prior to collapse was observed. Unfortunately, no visual inspection of these models was made during the tests.

The collapse pressures of Models SSS-14 through SSS-17, which are listed in Table 5, represent the pressures at which overall collapse occurred. However, visual inspection of the interior contour of these models indicated that excessive local deformation of the shell between stiffeners occurred during the test of each model. This excessive deformation was first observed at 1100, 1225, 775, and 500 psi for Models SSS-14, SSS-15, SSS-16, and SSS-17, respectively. Photographs of the progressive "buckling" of Model SSS-16 are presented in Figure 9.

The pressure load was applied to Model SSS-17 in four cycles. The first cycle reached a maximum pressure of 525 psi, the second cycle, 575 psi; the third cycle, 625 psi; and the final cycle reached the collapse pressure of 870 psi. When the pressure was removed at the end of the

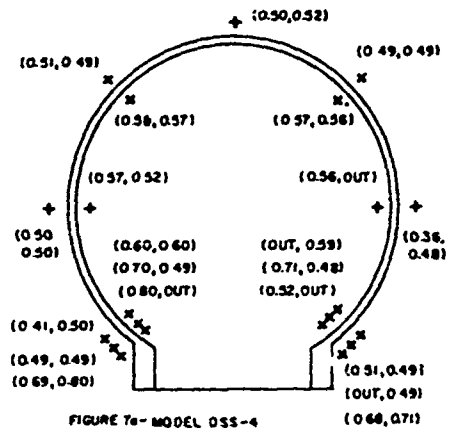

FIGURE 7a – MODEL DSS-4

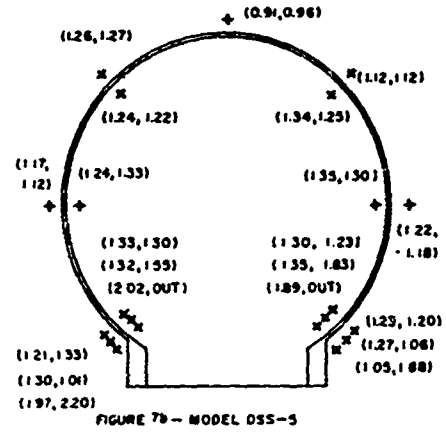

FIGURE 7b – MODEL DSS-5

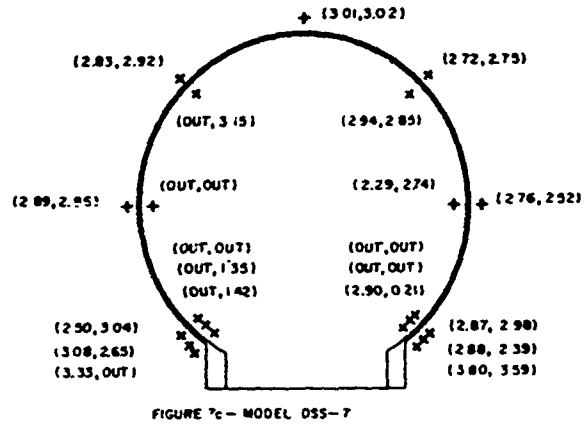

FIGURE 7c – MODEL DSS-7

Sensitivities are given in microinches per inch per psi. Circumferential sensitivities are listed first.

Figure 7 - Measured Strain Sensitivities for Series DSS, Models DSS-4, DSS-5, and DSS-7

first cycle, no permanent deformation was observed. Thus, the lobe which appeared at 500 psi in the thinnest shell segment of Model SSS-17 was essentially elastic at 525 psi. After the second cycle, some permanent deformation was observed at the location of the initial lobe. At the maximum pressure of the third cycle, a second lobe was observed. When the pressure was removed at the end of the third cycle, permanent deformation was observed at the location of both of the first two lobes. During

Figure 8 - Pressure versus Strain for Series DSS, Models DSS-4, DSS-5, and DSS-7

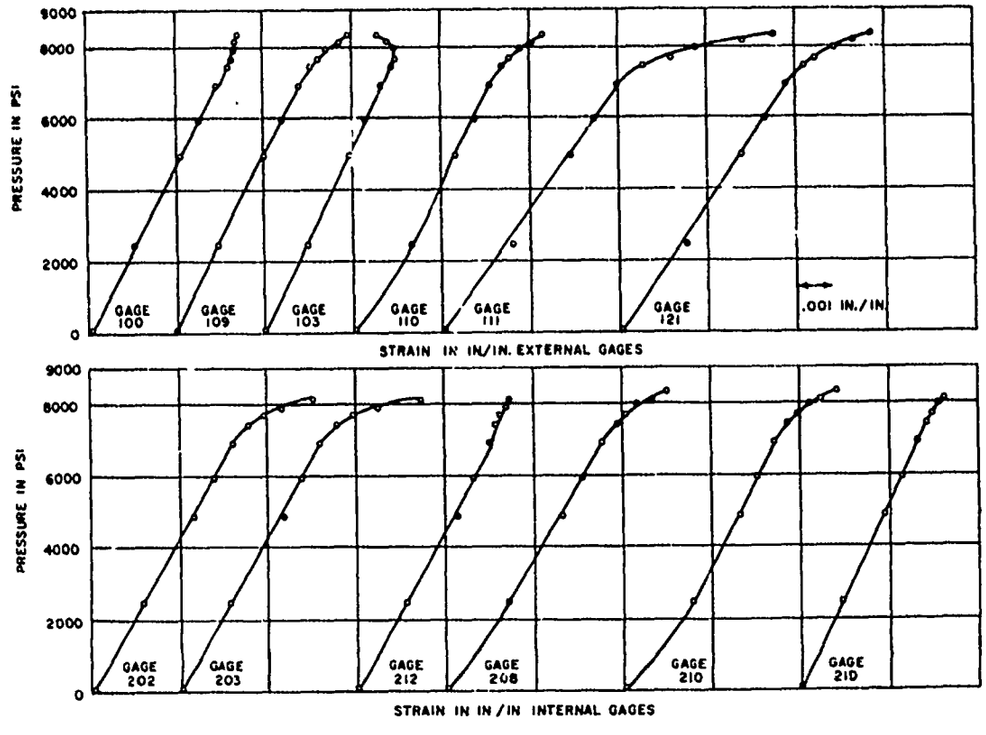

Figure 8a - Model DSS-4

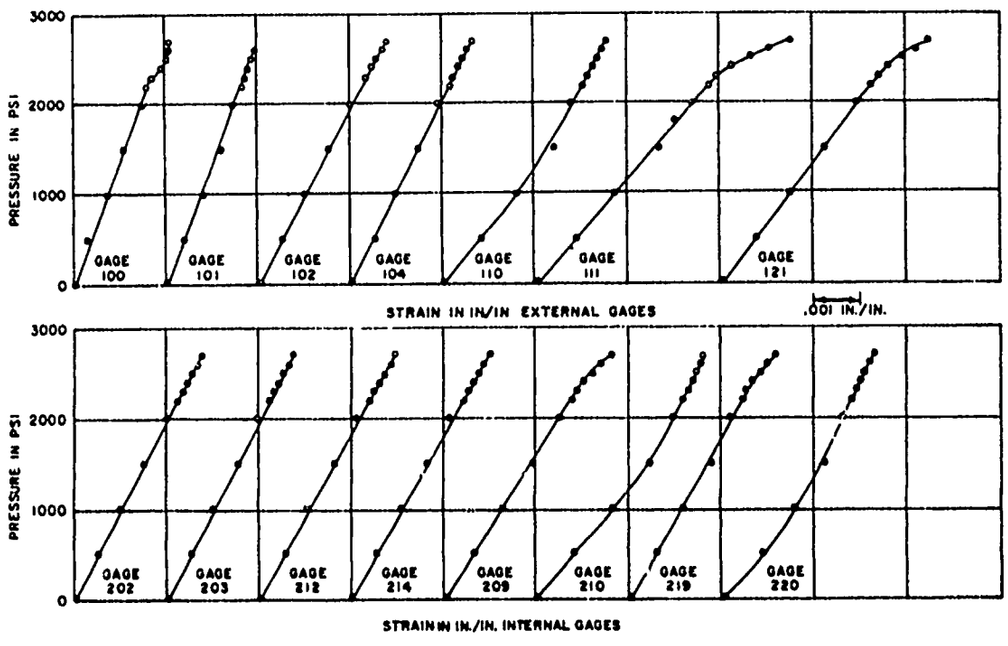

Figure 8b - Model DSS-5

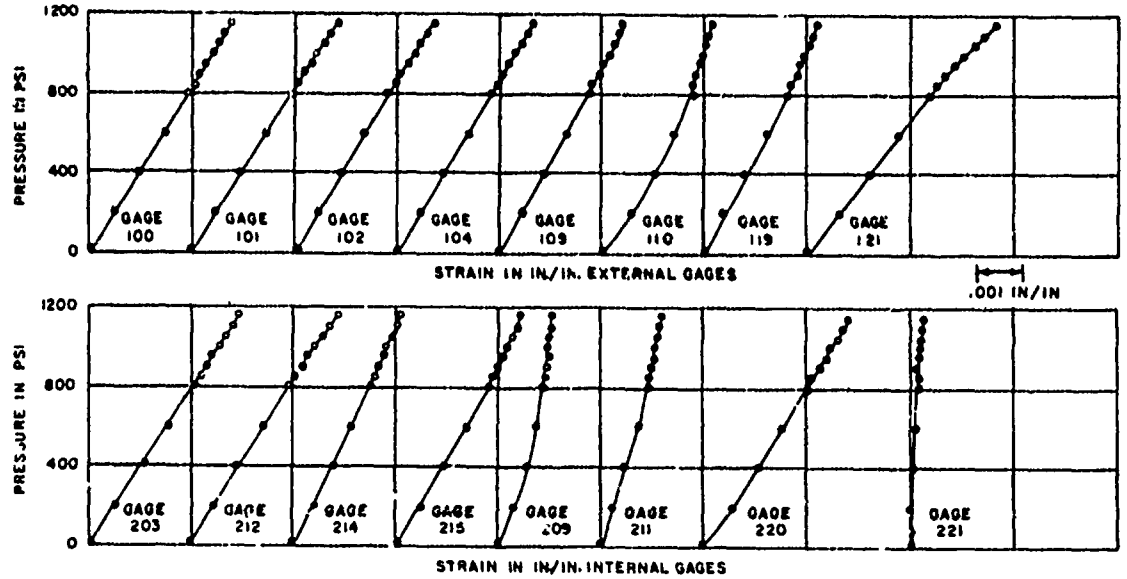

Figure 8c - Model DSS-7

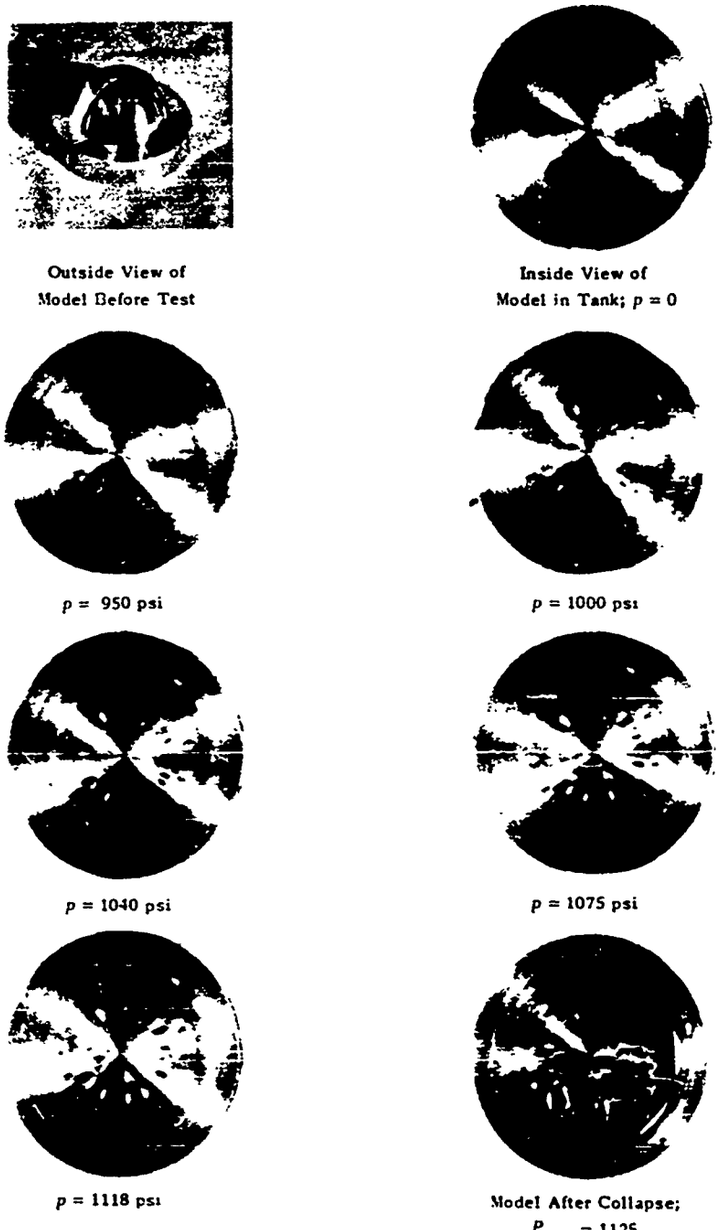

Outside View of Model Before Test

Inside View of Model in Tank; $p = 0$

$p = 950$ psi

$p = 1000$ psi

$p = 1040$ psi

$p = 1075$ psi

$p = 1118$ psi

Model After Collapse; $P_{exp} = 1125$

Figure 9 - Progressive Buckling of Model SSS-16

the final cycle, the number of lobes increased with increasing pressure until, immediately prior to collapse, nearly each segment of shell between stiffeners had formed an inward lobe.

DISCUSSION

SERIES S

Failure of each of the four Series S models occurred in regions removed from the hatch (see Figure 4a). It appears that increasing the thickness of the hatch cover and adjacent area by 10 percent eliminated failure of this region. In addition, the photographs of the collapsed models indicate that the failure occurred in regions unaffected by the hatch. This is particularly true for Models S-1 and S-3. Thus, the collapse strengths of the Series S models represent the collapse strengths of complete machined spheres. Unfortunately, no strain data were recorded during the tests so no conclusions can be made regarding the elastic behavior in way of the hatches.

TABLE 6

Summary of Geometric Parameters and Collapse Pressures for Series S Models

MODEL	ϕ deg	P_{exp} psi	σ_{avg} psi	P_3 psi	P_E psi	$\frac{P_3}{P_E}$	$\frac{P_{exp}}{P_E}$
S-1	360	14,300	84,300	70,260	14,150	5.05	1.01
S-2	360	8,500	76,500	29,530	8,720	3.40	0.98
S-3	360	3,000	62,300	5,355	3,400	1.58	0.88
S-4	360	1,500	58,300	1,495	1,465	1.02	1.02

Table 6 presents the average stresses of the Series S model at collapse calculated using Equation [7]. Each model collapsed at stress levels equal to or greater than the proportional limit of the material. Thus, each model collapsed by inelastic buckling.

Since the collapse of each model in Series S represented the inelastic buckling of a complete machined sphere, the empirical Equation [5] is considered applicable in calculating their collapse strength. It may be repeated that Equation [5] was suggested for use in calculating the inelastic as well as elastic buckling strength of machined deep spherical shells with ideal boundaries.[11] The experimental collapse pressures of these models are compared in Table 6 and Figure 10 with the pressures calculated by using Equation [5]. Table 6 also presents the empirical elastic buckling pressure calculated by using Equation [2] and indicates the relative stability of each model by presenting the ratio of the empirical elastic buckling pressure to the empirical inelastic buckling pressure. In addition, Figure 10 compares these present results with the earlier results of machined hemispheres with ideal boundaries.[11,12] The abscissa in Figure 10 is the ratio of the empirical buckling pressure p_E to p_1, the classical small-deflection elastic buckling pressure according to Equation [1] for $\nu = 0.3$; and the ordinate is the ratio of the experimental buckling pressure p_{exp} to p_1.

The agreement between the experimental results and the calculated values obtained from Equation [5] is excellent for Models S-1, S-2, and

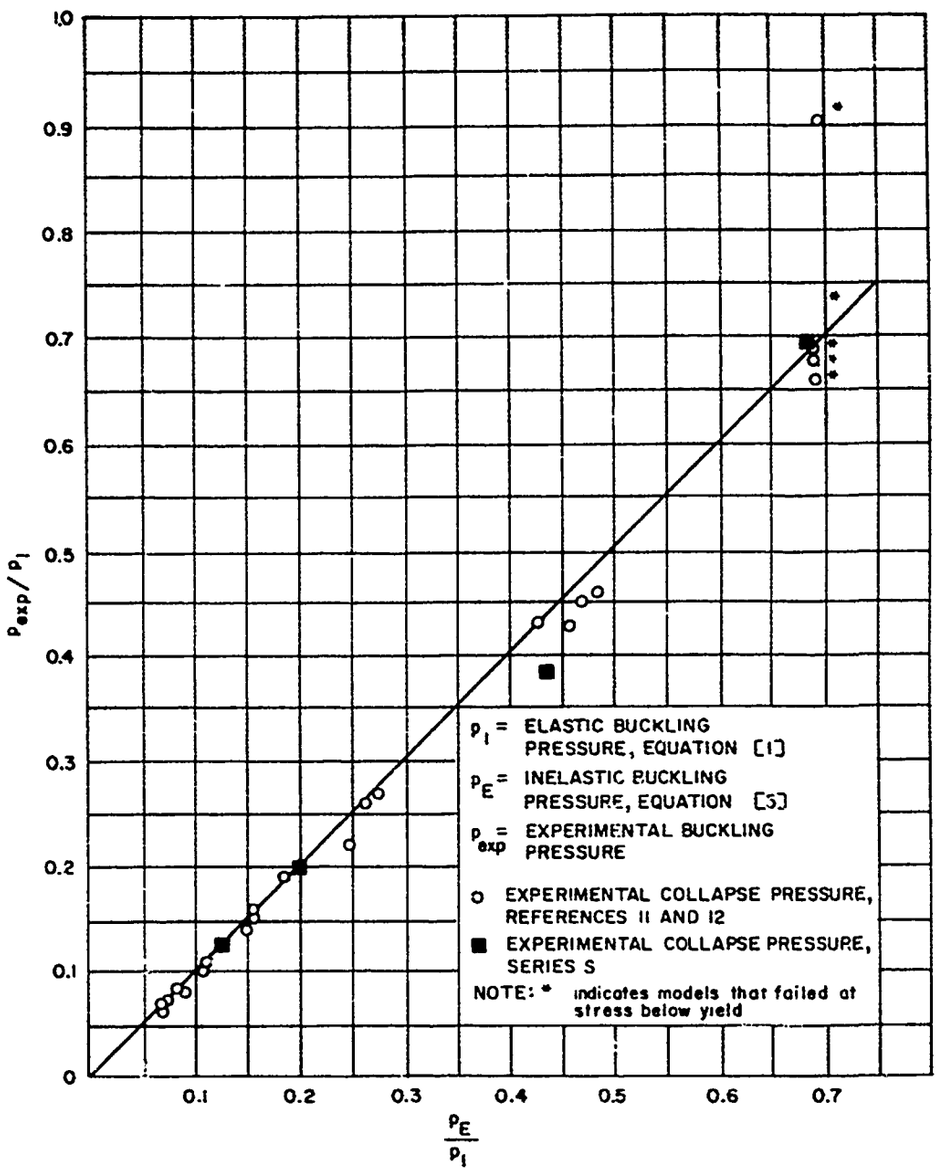

Figure 10 - Experimental Buckling Data for Machined Deep Spherical Shells with Ideal Boundaries

S-4. However, agreement between experimental and calculated pressures for Model S-3 was only fair; the experimental collapse pressure was about 12 percent below the calculated collapse pressure. Although this discrepancy may not appear to be very large, it is considerably greater than expected on the basis of earlier tests of machined shells[11] shown in Figure 10. There is no obvious explanation for this discrepancy; initial departures from sphericity may have lowered the experimental collapse pressure,* or a local reduction in the strength may have been present in the 7075-T6 aluminum bar stock.

Based on the results presented in Figure 10, Equation [5] adequately predicts the buckling strength of deep spherical shells with ideal boundaries machined to the accuracy represented by these models and the models presented in Reference 11. Unfortunately, the initial departure from sphericity was not measured for any of these shells. A quantitative picture of the departures from sphericity can be obtained, however, by studying the measured variations in thickness. Since none of the models were supported on the inside while final machining the outside contour, it seems unlikely that the initial departures from sphericity are any greater than the measured variations in wall thickness. Thus it appears that the spherical shells represented in Figure 10 had total initial departures from sphericity which were, in general, less than 5 percent of the shell thickness..

---

* The initial departures from sphericity were not measured for the Series S models but are assumed to be small since the shells were machined.

For design purposes, Equation [5] may be expected to adequately predict both the elastic and inelastic collapse strength of deep spherical shells with ideal boundaries or "complete spherical shells" whose contours have been accurately machined to ensure local variations in radii of less than 2 1/2 percent of the shell thickness[13] over a critical length. Accurately machined spherical shells may buckle elastically at pressures approaching 43 percent greater than the pressures obtained from Equation [5].[12] For design purposes, however, it appears unrealistic to rely on this additional strength.[12] This is caused to a great extent by the inability to measure the contours to the required degree of accuracy since most practical shells which fail elastically have low ratios of thickness to radius. Accurately machined shells which collapse in the inelastic region may also fail at pressures higher than those calculated by using Equation [5]. As in the case of the shells which fail elastically, however, it does not appear practical to rely on any strength in addition to that obtained from Equation [5].

If appreciable initial departures from sphericity are present, both the elastic and inelastic collapse strength of deep spherical shells with ideal boundaries will be lower than the pressure calculated by using Equation [5]. For design purposes, Equation [5] represents an upper bound for experimental collapse strength. If the initial departure from sphericity over a critical length is greater than about 2 1/2 percent of the shell thickness, the collapse strength will most likely be less than that

calculated using Equation [5]. A semi-empirical design approach for shells with initial departures in sphericity is presented in Reference 13.

The effects of variations in thickness, adverse boundary conditions and penetrations, and residual stresses are not considered in the development of Equation [5]. Therefore, caution must be exercised when using this design equation to ensure that none of these effects are present in the structure.

SERIES SS

The collapse pressures of those shallow spherical segment models which failed elastically (Models SS-25, SS-26, SS-33 through SS-36, and SS-57 through SS-73) are compared in Figure 11 with test results recorded in the literature[4,7,26,30] and with nonlinear axisymmetric theory.[23,24,25] The ordinate is the ratio of the experimental collapse pressure p_{exp} to p_3, the empirical elastic buckling pressure for machined deep spherical shells with membrane boundaries. The abscissa is the nondimensional geometric parameter θ^* defined as

$$\theta = \left[\frac{3}{4}(1-\nu^2)\right]^{1/4} \frac{L_a}{\sqrt{Rh}} = \frac{0.91\, L_a}{\sqrt{Rh}} \quad \text{for } \nu = 0.3 \qquad [8]$$

where L_a is the unsupported arc length of spherical shell.

Figure 11 also shows the results for four thin hemispherical shells with rigid boundaries[35] recently tested at the Model Basin. A summary

* It can be shown that θ is identical to the parameter μ used by Weinitschke[24] and others.

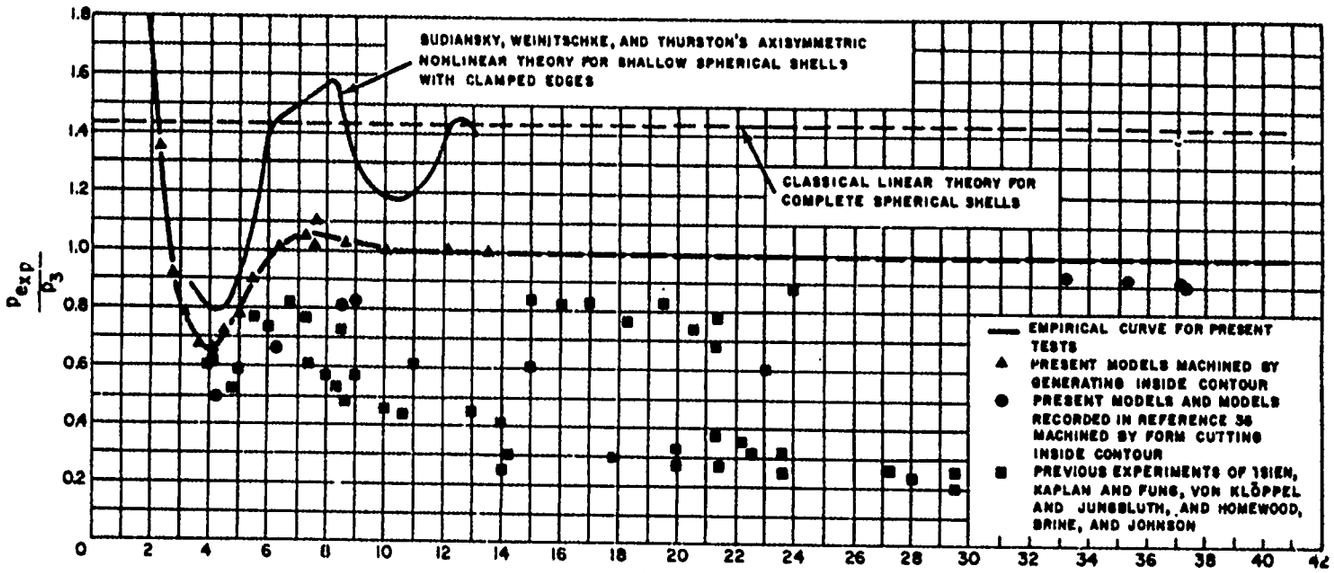

Figure 11 - Experimental Elastic Buckling Data for Spherical Shells with Clamped Edges

of geometric parameters and collapse pressures for each of the Series SS models is given in Table 7.

TABLE 7

Summary of Geometric Parameters and Collapse Pressures for Series SS Models

MODEL	ϕ deg	θ	P_{exp} psi	σ_{avg} psi	P_3 psi	P_E psi	$\frac{P_3}{P_E}$	$\frac{P_{exp}}{P_E}$
SS-1	120	6.21	14,175	82,605	73,200	14,320	5.11	0.99
SS-2	120	6.22	14,250	83,310	72,710	14,050	5.18	1.01
SS-3	120	8.51	8,500	74,815	31,290	8,950	3.50	0.95
SS-4	120	7.84	8,175	73,290	29,910	8,710	3.43	0.94
SS-5	120	12.19	2,900	60,790	5,290	3,370	1.56	0.86
SS-6	120	12.26	2,950	62,430	5,180	3,350	1.55	0.88
SS-7	120	17.06	1,100	44,640	1,395	1,395	1.00	0.79
SS-8	120	17.15	1,090	44,665	1,365	1,365	1.00	0.80
SS-9	60	3.09	14,375	83,130	73,380	14,850	5.00	0.97
SS-10	60	3.11	14,225	82,975	73,040	14,360	5.08	0.99
SS-11	60	3.90	8,200	72,695	30,600	8,920	3.43	0.92
SS-12	60	3.89	8,100	71,685	30,700	8,900	3.45	0.91
SS-13	60	6.02	2,925	59,885	5,540	3,480	1.59	0.84
SS-14	60	6.05	2,875	59,415	5,440	3,420	1.59	0.84
SS-15	60	8.54	1,070	43,420	1,390	1,390	1.00	0.77
SS-16	60	8.54	1,080	43,825	1,390	1,390	1.00	0.78
SS-17	45	2.32	18,400	106,410	74,460	13,800	5.40	1.33
SS-18	45	2.33	18,200	106,055	73,200	13,620	5.37	1.34
SS-19	45	2.90	8,700	76,165	31,420	8,750	3.59	0.99
SS-20	45	2.91	8,320	73,365	30,940	8,690	3.54	0.96
SS-21	45	4.50	2,480	50,305	5,650	3,450	1.65	0.72
SS-22	45	4.52	2,545	51,860	5,600	3,390	1.65	0.75
SS-23	45	6.32	1,060	42,005	1,460	1,460	1.00	0.73
SS-24	45	6.35	1,055	42,200	1,435	1,435	1.00	0.74
SS-25	45	8.56	355	25,565	439	439	1.00	0.81
SS-26	45	9.04	290	23,315	352	352	1.00	0.82
SS-27	30	1.86	18,550	150,090	36,960	9,700	3.84	1.91
SS-28	30	1.86	18,375	149,290	36,650	9,610	3.81	1.91
SS-29	30	1.94	16,320	143,500	31,120	8,790	3.54	1.86
SS-30	30	1.94	15,930	140,850	30,760	8,700	3.54	1.83
SS-31	30	3.03	2,725	56,450	5,410	3,410	1.59	0.80
SS-32	30	3.03	2,700	55,800	5,440	3,400	1.60	0.79
SS-33	30	4.19	735	28,720	1,500	1,500	1.00	0.49

TABLE 7 (Cont'd)

MODEL	ϕ deg	θ	p_{exp} psi	σ_{avg} psi	p_3 psi	p_E psi	$\frac{p_3}{p_E}$	$\frac{p_{exp}}{p_E}$
SS-34	30	4.25	685	27,530	1,420	1,420	1.00	0.48
SS-35	30	6.15	270	22,585	326	326	1.00	0.83
SS-36	30	6.28	195	17,180	294	294	1.00	0.66
SS-37	20	1.60	14,375	189,860	13,520	5,880	2.30	2.45
SS-38	20	1.61	14,250	189,340	13,360	5,830	2.29	2.45
SS-39	20	2.13	4,350	99,835	4,390	3,100	1.42	1.40
SS-40	20	2.16	4,150	97,655	4,180	3,010	1.39	1.38
SS-41	20	2.97	945	41,640	1,180	1,180	1.00	0.80
SS-42	20	2.93	950	41,020	1,230	1,230	1.00	0.77
SS-43	10	1.30	-	-	2,000	1,890	1.06	-
SS-44	10	1.31	-	-	1,955	1,845	1.06	-
SS-45	10	1.49	-	-	1,175	1,175	1.00	-
SS-46	10	1.48	-	-	1,190	1,190	1.00	-
SS-47	10	1.64	-	-	799	799	1.00	-
SS-48	10	1.66	-	-	754	754	1.00	-
SS-49	5	1.37	-	-	164	164	1.00	-
SS-50	5	1.37	-	-	165	165	1.00	-
SS-51	5	1.54	-	-	103	103	1.00	-
SS-52	5	1.54	-	-	103	103	1.00	-
SS-53	5	1.79	-	-	56.4	56.4	1.00	-
SS-54	5	1.84	-	-	49.9	49.9	1.00	-
SS-55	5	2.61	-	-	17.1	17.1	1.00	-
SS-56	5	2.61	-	-	17.1	17.1	1.00	-
SS-57	16.5	2.28	2,050	78,000	1,540	1,540	1.00	1.33
SS-58	18.5	2.73	1,080	47,000	1,175	1,175	1.00	0.92
SS-59	20.0	3.19	690	34,700	878	878	1.00	0.79
SS-60	22.8	3.64	605	30,200	894	894	1.00	0.68
SS-61	25.7	4.10	580	29,100	883	883	1.00	0.66
SS-62	25.7	4.10	570	28,500	889	889	1.00	0.64
SS-63	23.4	4.45	290	21,700	398	398	1.00	0.73
SS-64	25.7	5.01	312	23,400	398	398	1.00	0.79
SS-65	24.3	5.46	193	19,700	215	215	1.00	0.89
SS-66	32.4	7.28	225	23,000	215	215	1.00	1.05
SS-67	32.4	7.51	218	23,300	199	199	1.00	1.10
SS-68	28.1	6.30	226	22,700	225	225	1.00	1.00
SS-69	38.1	8.67	213	21,400	207	207	1.00	1.03
SS-70	46	10.0	257	24,150	257	257	1.00	1.00
SS-71	54	12.1	249	21,800	247	247	1.00	1.08
SS-72	60	13.5	246	21,500	247	247	1.00	1.00
SS-73	35.2	7.61	245	24,600	243	243	1.00	1.00

The interior contours of all the machined models represented in Figure 11, except Models SS-57 through SS-73, were obtained by use of the form tool. Erratic results were obtained from each of the models obtained by form tool except for those models recorded in Reference 35. These erratic results were undoubtedly caused by initial departures from sphericity. Unfortunately, no measurements were made of the initial contours. It appears that the inside contours of these models, which were very thin, were not perfectly spherical. Under the pressure of the tool, however, these interior contours conformed to the spherical surface of the support mandrel while the exterior contours were final machined. When the machining operations were completed and the model was removed from the support mandrel, these models apparently assumed the shape of the inside contours. Thus, a uniform wall thickness was obtained although initial departures from sphericity were present in the shell after machining.

Like previous experiments recorded in the literature, the present tests of models machined by use of a form tool showed a complete lack of repeatability. However, the present results of models machined by generating both inside and outside contours followed a very definite pattern (see Figure 11). Models SS-57 through SS-73 each had near-perfect sphericity; the variation in measured local inside radii for each of these models was less than 0.0002 in. and normally less than 0.0001 in. Therefore, as in the case of the machined deep spherical shells with

favorable boundaries, these results demonstrate the detrimental effects of initial departure from sphericity on collapse strength. These results also demonstrate that a small clamped segment can be weaker than a larger clamped segment. Although this phenomenon has been implied by existing theoretical studies, it found no support in the earlier experiments and several investigators have stated that it is physically not feasible.[29,36] An obvious implication of these results is that stiffening systems may weaken rather than strengthen a spherical shell if placed at critical spacings.

The empirical curve arbitrarily drawn through the experimental points in Figure 11 has the same general shape as the theoretical curve of Budiansky,[23] Weinitschke,[24] and Thurston[25] for short segments associated with values of θ less than about 5.5. However, as the shells become longer or deeper, the empirical curve departs from the theoretical curve. Since the theoretical curve represents collapse pressures in the symmetric mode, it is reasonable to assume that the mode of collapse becomes nonsymmetric in this region. Actually, the deformed surfaces of the three longest generated segments after collapse were nonsymmetric in nature, whereas the others were symmetric. This does not necessarily mean that all of the 14 shallower segments failed in the symmetric mode. Previous investigators[4,30] have found that failures which appear to be symmetric after collapse may have initiated in the nonsymmetric mode.

Weinitschke recently developed a theory for the nonsymmetric buckling of shallow spherical shells.[32] Although his theory is in fair agreement with early experiments, it completely disagrees with the present results. Assuming that the same degree of accuracy was achieved in all of the 17 generated models, it appears that the correct theoretical nonsymmetric buckling pressure for clamped segments would be critical for values of θ greater than about 5.5 and would be equal to roughly 80 to 90 percent of the classical buckling pressure for complete spheres.*

Models SS-43 through SS-56 did not buckle nor did they collapse or rupture under external pressure (see Figures 5 and 6). Each of these models had thickness-to-radius ratios which would ensure elastic buckling if in the form of complete spheres. However, each shell was extremely shallow with included angles of 5 to 10 deg whereas the smallest included angle for the shells that did buckle was 16 1/2 deg. Most of these shells also had extremely small values of θ. Either of these factors might preclude buckling. The preliminary analysis on these models however, is not sufficient to reach any definite conclusions.

The test results of those models which failed at stress levels above the proportional limit of the material σ_p are presented in Figure 12 as a function of the geometric parameter ϑ. The results are quite consistent when plotted in contour of ratios of p_3 to p_E. For those deep segments

* In discussing Weinitschke's paper[32] at the recent NASA Symposium on Instability of Shell Structures, Budiansky indicated that his early theoretical results follow this same general pattern.

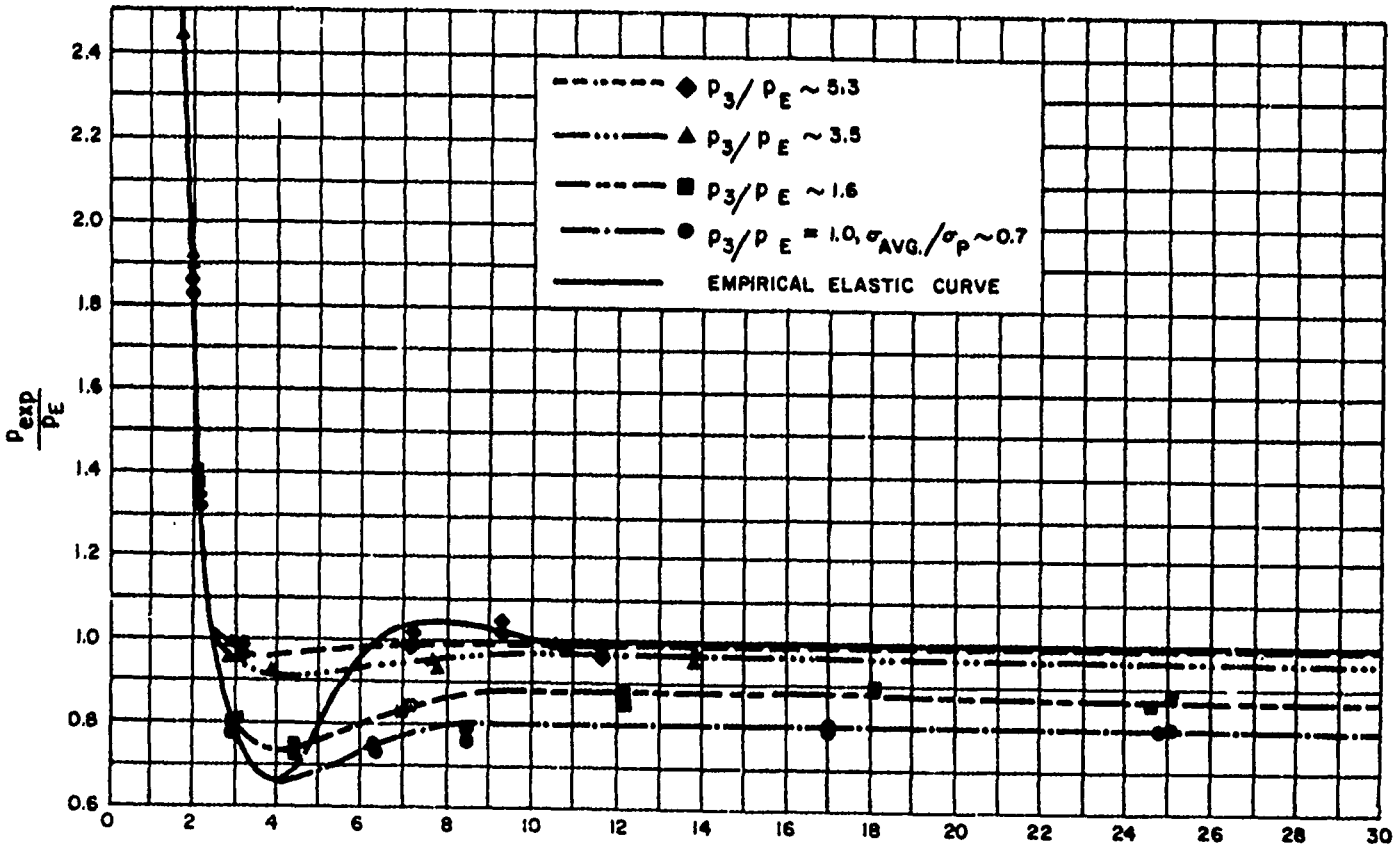

$$\theta = \left[\frac{3}{4}(1-\nu^2)\right]^{1/4} \frac{L_a}{\sqrt{Rh}} = 0.91 \frac{L_a}{\sqrt{Rh}} \text{ for } \nu = 0.3$$

Figure 12 - Experimental Inelastic Buckling Data for Spherical Shells with Clamped Edges

which had ratios of p_3 to p_E of 1 but had membrane stresses of collapse (σ_{avg}) of about 70 percent of the proportional limit, the observed collapse strength was about 20 percent less than would be expected for a near-perfect complete sphere or a deep machined sphere with ideal boundaries. As the ratio of p_3 to p_E increased (that is, as the shell became more stable), the effects of clamping the edges diminished for all except the very shallow, or short, shells.

Regardless of the ratio of p_3 to p_E, the buckling strength of all segments increased rapidly for descending values of θ below about 2.2 to 2.5. Therefore, it is apparent that stiffeners must be placed at relatively close intervals in order to realize an increase in either elastic or inelastic buckling strength. Placing stiffeners at spacings greater than the arc length corresponding to a θ of about 2.5 will not increase the local buckling strength of the shell and may possibly weaken it.

Another, more abstract conclusion obtained from these tests is related to initial departures from sphericity or local "flat spots." If a spherical shell contains a flat spot covering an arc length associated with a θ of about 2.2 or greater, the collapse strength of this shell would appear to be relatively independent of the nominal radius of the shell. Based on the local curvature of the "flat spot" rather than on the nominal curvature which is commonly used, a new upper bound may be determined for the collapse strength of an initially imperfect spherical shell. This observation is the basis of an analysis developed in Reference 13 which

adequately predicts both the elastic and inelastic strength of 36 machined models with local flat spots covering a relatively wide range of θ.

A stress analysis should be conducted on the Series SS shells as well as on the other shells reported herein to more fully understand their behavior. It is anticipated that this will be undertaken in the near future.

SERIES DSS

Failure of each of the Series DSS models except the two thinnest models (DSS-7 and DSS-8) occurred away from the boundary (see Figure 4). Thus, the boundary conditions did not have a severe effect on collapse. This conclusion is supplemented by the strain data presented in Figures 7 and 8. The strain sensitivities plotted in Figure 7 show that the edge effects did not cause excessive strains at the shell-boundary ring juncture. It appears that these relatively low strains were primarily the result of the taper at the juncture. Figure 8 shows that during the test there was a change in the slope of the pressure-strain plots of gages adjacent to the boundary ring. This indicates that the solid plug placed inside the opening was not fitted sufficiently tight to support the boundary ring during the early stages of the loading cycle. This also may have reduced the boundary effects.

Since the boundary conditions of the Series DSS models were not severe, the empirical formula for near-perfect spheres should be applicable in calculating their collapse strength. Table 8 compares the experimental collapse pressures with the collapse pressures calculated

TABLE 8

Summary of Geometric Parameters and Collapse Pressures for Series DSS Models

MODEL	ϕ deg	θ	p_{exp} psi	σ_{avg} psi	p_3 psi	p_E psi	$\frac{p_3}{p_E}$	$\frac{p_{exp}}{p_E}$
DSS-1	300	17.20	11,100	74,925	49,780	10,800	4.61	1.03
DSS-2	300	16.84	11,375	74,630	52,690	11,660	4.52	0.98
DSS-3	300	25.57	4,720	69,310	10,520	4,810	2.19	0.98
DSS-4	300	19.38	8,400	73,565	31,390	8,420	3.73	1.00
DSS-5	300	30.21	2,800	57,555	5,500	3,250	1.69	0.86
DSS-6	300	30.84	2,925	64,305	4,800	2,975	1.61	0.98
DSS-7	300	44.95	1,200	54,470	1,113	1,070	1.04	1.12
DSS-8	300	42.73	1,290	52,985	1,360	1,330	1.02	0.97

by using the empirical formula. Good agreement was obtained for each model except DSS-5 and DSS-7 which were relatively unstable shells. Model DSS-5 collapsed at a pressure 14 percent less than the calculated pressure, and Model DSS-7 collapsed at a pressure 12 percent above the calculated pressure. As in the case of Model S-3, the relatively low collapse pressure of Model DSS-5 may most likely be attributed to the presence of local departures from sphericity or to a local reduction in the strength of the 7075-T6 aluminum bar stock. The high collapse pressure of Model DSS-7 is rather surprising in view of the fact that its strength was most likely reduced at least a small amount by the edge condition. Thus, it is apparent that the sphericity of Model DSS-7 was extremely good. Unfortunately, no measurements were made of its initial contour. However, this high collapse pressure of Model DSS-7 once again lends support to the validity of the classical theory when applied to perfect spheres.

SERIES SSS

The experimental collapse pressures of the Series SSS stiffened shells are compared in Table 9 with the estimated collapse strength of the shells, neglecting the stiffeners and the estimated collapse strength of equivalent unstiffened shells of the same weight. Although installing stiffeners at sufficiently close intervals increased the collapse strength of the spherical shells, in no case was the collapse strength of the stiffened shell as great as would be expected for a machined unstiffened shell of the same weight.

These tests were rather exploratory in nature and they do not by any means demonstrate that effective stiffening systems cannot be developed. They do demonstrate, however, that certain types of stiffening systems will not be effective. In so doing, these Series SSS tests support the conclusion drawn from the Series SS tests; i.e., stiffeners must be placed at relatively close intervals in order to increase the collapse strength of a spherical shell. Each model having an unsupported arc length corresponding to values considerably in excess of 2.2 collapsed at a pressure below that calculated for the unstiffened shell. These models were SSS-1, SSS-2, and SSS-10 through SSS-13. The remaining models had relatively short unsupported arc lengths. Of these, the circumferentially stiffened Models SSS-3 through SSS-9 had no increase in strength or had only a marginal increase in strength over that predicted for the respective shells, neglecting the stiffeners. However, the appearance of

TABLE 9

Comparison of Experimental Collapse Pressures of Stiffened Models with Estimated Collapse Pressures for Unstiffened Spheres of the Same Weight

MODEL	Stiffener Type*	p_{exp} psi	$\frac{h}{R_o}$	p_3 psi	$\frac{p_{exp}}{p_3}$	p_E psi	$\frac{p_{exp}}{p_E}$	$\frac{h_e}{R_o}$**	p_3'*** psi	$\frac{p_{exp}}{p_3'}$	p_E' psi	$\frac{p_{exp}}{p_E'}$
SSS-1	1	1100	0.01275	1475	0.75	1437	0.76	0.01502	2045	0.54	1850	0.60
SSS-2	1	875	0.01083	1064	0.82	1064	0.82	0.01311	1555	0.56	1505	0.58
SSS-3	1	700	0.00902	738	0.95	738	0.95	0.01244	1405	0.50	1390	0.50
SSS-4	1	920	0.01071	1041	0.88	1048	0.88	0.01526	2115	0.44	1905	0.48
SSS-5	1	950	0.00938	798	1.19	798	1.19	0.01418	1825	0.52	1705	0.56
SSS-6	1	930	0.00938	798	1.17	798	1.17	0.01409	1800	0.52	1690	0.55
SSS-7	1	915	0.00926	778	1.18	778	1.18	0.01397	1770	0.52	1665	0.55
SSS-8	1	2740	0.01967	3510	0.78	2650	1.03	0.02423	5325	0.51	3440	0.80
SSS-9	1	2390	0.01836	3060	0.78	2430	0.98	0.02294	4775	0.50	3200	0.75
SSS-10	2	265	0.00562	287	0.92	287	0.92	0.01107	1110	0.24	1110	0.24
SSS-11	2	290	0.00575	300	0.97	300	0.97	0.011198	1140	0.26	1140	0.26
SSS-12	2	435	0.00757	520	0.84	520	0.84	0.01881	3210	0.14	2510	0.17
SSS-13	2	825	0.01072	1042	0.79	1042	0.79	0.02057	3840	0.22	2810	0.29
SSS-14	3	1325	0.00944	809	1.64	809	1.64	0.02003	3640	0.36	1875	0.71
SSS-15	3	1345	0.00986	882	1.53	882	1.53	0.02076	3910	0.34	1815	0.74
SSS-16	3	1125	0.00830	625	1.80	625	1.80	0.02187	4340	0.26	1660	0.68
SSS-17	3	870	0.00627	356	2.44	356	2.44	0.01993	3600	0.24	1395	0.62

* 1. Stiffeners parallel to hemispherical openings, only
2. Meridional stiffeners, only
3. Both stiffeners parallel to opening and meridional stiffeners.

** h_e represents the shell thickness of an equivalent unstiffened sphere of the same weight.

*** Prime designates use of equivalent shell thickness in calculations.

these models after collapse suggests that their strength was affected by their boundary conditions. The models with both circumferential and meridional stiffeners (Models SSS-14 through SSS-17) were considerably stronger than predicted for the unstiffened portion only.

The benefits of stiffening in both the circumferential and meridional direction or in the circumferential direction only appear worthy of further investigation. This is particularly true for welded shells where the efficiency of unstiffened shells is considerably less than that of machined, unstiffened shells. However, due to the inefficient distribution of the material, the use of meridional stiffeners only shows little promise of producing successful results.

The main obstacle in achieving efficient stiffening systems stems from the resulting stress field which they produce. The stiffener resists load in its axial direction only whereas the hydrostatic loading causes, essentially, a uniform biaxial load to occur in an unstiffened spherical shell. Since the stiffener offers no resistance to load in the plane normal to the stiffener, it can be no more than half as efficient as the shell material if buckling is neglected. Thus if strain hardening and three-dimensional stress effects are neglected, the maximum pressure to be achieved from a spherical shell with stiffeners in one direction only is that pressure which, according to Equation [7], causes the stresses to reach the yield point of the material. For spherical shells uniformly stiffened in two directions, the maximum pressure to be achieved is that

pressure which causes the average stresses in the stiffener-shell combination to reach the yield point of the material. This pressure may be determined by substituting an equivalent thickness into Equation [7]. This equivalent thickness is that of the shell and one stiffener only. The stiffeners accounted for 50 to 60 percent of the total material of Models SSS-14 through SSS-17. Since each of these models failed at stress levels beyond the proportional limit, it is not surprising that their collapse pressure was on the order of 30 percent less than that calculated for the unstiffened sphere of the same weight.

A stiffened spherical shell may buckle in various modes, depending on the stiffening system. Placing stiffeners in a single direction at relatively large intervals will have no strengthening effect on a spherical shell and may possibly have a slight weakening effect. A shell stiffened in this manner will most likely fail by the formation of a small inward lobe similar to the complete sphere. On the surface, it appears that the buckling of spherical shells with closely spaced stiffeners in only one direction is analogous to the axisymmetric buckling of short cylinders.[37] The buckling of those shells stiffened in two directions appears to be closely associated with the strength of spherical caps as demonstrated in Figures 11 and 12. In addition, however, the shell-stiffener combination of both types of stiffening systems may buckle, particularly if relatively small stiffeners are placed at extremely close intervals. It appears that a sandwich spherical shell would effectively resist this overall mode of

collapse and, thus, this shell is worthy of investigation. However, serious problems in fabrication and "inservice" inspection of sandwich spheres are visualized.

At the present time no theories are available for calculating the buckling strength or the stress distribution of stiffened spherical shells. It is apparent, therefore, that considerable study, both theoretical and experimental, is required before rational designs of efficient stiffened spheres may be achieved.

CONCLUSIONS

1. For design purposes, Equation [5] adequately predicts both the elastic and inelastic strength of initially stress-free complete spheres or of deep spheres with ideal boundaries whose local variations in radii are less than about 2 1/2 percent of the shell thickness.

2. Whereas previous experiments on shallow spherical shells with clamped edges recorded in the literature show a complete lack of repeatability, the present models follow a very definite pattern. However, no theory presently available in the literature may be used to adequately predict their behavior throughout the range investigated.

3. A spherical segment with an arc length associated with a value of the geometric parameter θ of about 2.2 or greater is not strengthened by its boundary. Thus, stiffeners must be placed at very close intervals in order to increase the strength of spherical shells. Similarly, the strength of an initially imperfect sphere is mainly dependent on the local curvature

over a "flat spot" of critical length rather than on the nominal curvature.

4. A small clamped spherical segment may be weaker than a larger clamped segment. Thus, stiffening systems may weaken rather than strengthen a spherical shell if placed at critical spacings.

5. Installing stiffeners in spherical shells at close intervals increases their experimental collapse strength.

6. In no case was the experimental collapse strength of a stiffened spherical shell as great as would be expected for a machined unstiffened shell of the same weight. These tests do not demonstrate, however, that effective stiffening systems cannot be developed.

ACKNOWLEDGMENTS

The authors acknowledge the significant contributions of Mr. Leonard Giuffreda who conducted the hydrostatic tests and Messrs. John Collier and George Junkin who assisted in the reduction and presentation of the data. The Industrial Department is commended for skill in machining the models to a very high degree of accuracy. In particular, the authors are indebted to Messrs. Chauncey Reed and Glenwood Cooper for supervising the machining processes.

REFERENCES

1. Abraham, L. H. and Lowy, M. J., "Shell Instability Problems as Related to Design," National Advisory Space Administration TN D-1510, p. 1 (Dec 1962).

2. Fung, Y. C. and Seckler, E. E., "Instability of Thin Elastic Shells," Proceedings of the First Symposium on Naval Structural Mechanics (1960).

3. Timoshenko, S., "Theory of Elastic Stability," McGraw-Hill Book Co., Inc., New York (1936).

4. Kloppel, K. and Jungbluth, O., "Beitrag zum Durchschlagsproblem Dunwandieger Kugelschalen (Versuche und Bemessungsformeln), (Contribution to the Durchschlag-Problem in Thin-Walled Spherical Shells (Experiments and Design Formulas)," Der Stahlbau, Jahrg. 22, Heft 6, Berlin (1953).

5. Von Kármán, T. and Tsien, H. S., "The Buckling of Spherical Shells by External Pressure," Journal of the Aeronautical Sciences, Vol. 7, No. 2 (Dec 1939).

6. Friedrichs, K. O., "On the Minimum Buckling Load for Spherical Shells," Theodore von Karman Anniversary Volume, California Institute of Technology (1941).

7. Tsien, H. S., "A Theory for the Buckling of Thin Shells," Journal of the Aeronautical Sciences, Vol. 9, No. 10 (Aug 1942).

8. Yoshimura, Y. and Uemura, M., "The Buckling of Spherical Shells Due to External Pressures," Reports, Institute of Science and Technology, University of Tokyo, Vol. 3, p. 316 (1949).

9. Thompson, J. M. T., "The Elastic Instability of a Complete Spherical Shell," The Aeronautical Quarterly (May 1962).

10. Wedellsborg, B. W., "Critical Buckling Load on Large Spherical Shells," Journal of the Structural Division, ASCE, Vol. 88, No. ST1 (Feb 1962).

11. Krenzke, M. A., "Tests of Machined Deep Spherical Shells under External Hydrostatic Pressure," David Taylor Model Basin Report 1601 (May 1962).

12. Krenzke, M. A., "The Elastic Buckling Strength of Near-Perfect Deep Spherical Shells with Ideal Boundaries," David Taylor Model Basin Report 1713 (Jul 1963).

13. Krenzke, M. A. and Kiernan, T. J., "The Effect of Initial Imperfections on the Collapse Strength of Deep Spherical Shells," David Taylor Model Basin Report 1757 (in preparation).

14. Bijlaard, P. P., "Theory and Tests on the Plastic Stability of Plates and Shells," Journal of the Aeronautical Sciences, Vol. 16, No. 9 (Sep 1949).

15. Gerard, G., "Plastic Stability Theory of Thin Shells," Journal of the Aeronautical Sciences, Vol. 24, No. 4 (Apr 1957).

16. Lunchick, M. E., "Plastic Buckling Pressure for Spherical Shells," David Taylor Model Basin Report 1493 (Jul 1963).

17. Kiernan, T. J., "The Buckling Strength of Segmented HY-80 Steel Hemispheres," David Taylor Model Basin Report 1721 (in preparation).

18. Krenzke, M. A., "Hydrostatic Tests of Conical Reducers between Cylinders with and without Stiffeners at the Cone-Cylinder Junctures," David Taylor Model Basin Report 1187 (Feb 1959).

19. Krenzke, M. A. and Kiernan, T. J., "Structural Development of a 15,000- to 20,000-Foot Titanium Oceanographic Vehicle," David Taylor Model Basin Report 1677 (Sep 1963).

20. Kiernan, T. J. and Krenzke, M. A., "Experimental Investigation of Closures and Penetrations for Pressure Vessels of Composite Construction," David Taylor Model Basin Report 1732 (in preparation).

21. Nott, J. A., "Structural Design of Viewing Ports for Oceanographic Vehicles," David Taylor Model Basin Report 1737 (Mar 1963).

22. Feodosiev, V. I., "Calculation of Thin Clicking Membranes," Prikladnaia Matematika i Mekhanika, Vol. X, p. 295 (1946).

23. Budiansky, B., "Buckling of Clamped Shallow Spherical Shells," Proceedings of the I.V.T.A.M. Symposium of the Theory of Thin Elastic Shells, North Holland Publishing Company, Amsterdam, p. 64 (1960).

24. Weinitschke, H., "On the Stability Problem for Shallow Spherical Shell," Journal of Mathematics and Physics, Vol. 38, No. 4, p. 209 (Jan 1960).

25. Thurston, G. A., "A Numerical Solution of the Non-Linear Equations for Axisymmetric Bending of Shallow Spherical Shells," Journal of Applied Mechanics, Vol. 28, No. 4, p. 557 (Dec 1961).

26. Kaplan, A. and Fung, Y. C., "A Non-Linear Theory of Bending and Buckling of Thin Elastic Shallow Spherical Shells," National Advisory Committee for Aeronautics TN 3212 (Aug 1954).

27. Reiss, E. L., et al., "Non-Linear Deflections of Shallow Spherical Shells," Journal of the Aeronautical Sciences, Vol. 54, p. 533 (Jul 1957).

28. Archer, R. R., "Stability Limits for a Clamped Spherical Shell Segment under Uniform Pressures," Quarterly of Applied Mathematics, Vol XV, p. 355 (Jan 1958).

29. Von Willich, G. P. R., "The Elastic Stability of Thin Spherical Shells," Journal of the Engineering Mechanics Division, Proceedings of the American Society of Civil Engineers, Vol. 185, No. EM.1 (Jan 1959).

30. Homewood, R. H., et al., "Experimental Investigation of the Buckling Instability of Monocoque Shells," Experimental Mechanics, Vol. 1, No. 3, p. 88 (Mar 1961).

31. Chen, W. L., "Effect of Geometrical Imperfections on the Elastic Buckling of Shallow Spherical Shells," Sc.D. Thesis, Department of Civil and Sanitary Engineering, Massachusetts Institute of Technology (Jan 1959).

32. Weinitschke, H., "Asymmetric Buckling of Clamped Shallow Spherical Shells," National Advisory Space Administration TN D-1510, p. 481 (Dec 1962).

33. Hodge, P. G., "Plastic Analysis of Structures," McGraw-Hill Book Co., Inc., New York (1959).

34. Roth, R. S., "Plastic Buckling of Thin Shallow Spherical Shells," Division of Engineering and Applied Physics, Harvard University Technical Report No. 13 (May 1962).

35. Kiernan, T. J., "The Effects of Boundary Conditions on the Collapse Strength of Machined Hemispherical Shells under External Hydrostatic Pressure," David Taylor Model Basin Report (in preparation).

36. Klein, B., "Further Remarks on the Collapse Pressure of Uniformly Loaded Spherical Shells," Journal of the Aeronautical Sciences, Vol. 24, p. 309 (1957).

37. Lunchick, M. E., "Plastic Axisymmetric Buckling of Ring-Stiffened Cylindrical Shells Fabricated from Strain-Hardening Materials and Subjected to External Hydrostatic Pressure," David Taylor Model Basin Report 1393 (Jan 1961).

INITIAL DISTRIBUTION

Copies	
15	CHBUSHIPS
	2 Sci & Res (Code 442)
	1 Lab Mgt (Code 320)
	3 Tech Lib (Code 210L)
	1 Struc Mech, Hull Mat & Fab (Code 341A)
	1 Prelim Des Br (Code 420)
	1 Prelim Des Sec (Code 421)
	1 Ship Protec (Code 423)
	1 Hull Des Br (Code 440)
	1 Struc Sec (Code 443)
	2 Sub Br (Code 525)
	1 Pres Ves Sec (Code 651F)
2	CHONR
	1 Struc Mech Br (Code 439)
	1 Undersea Programs (Code 466)
4	CNO
	1 Plans, Programs & Req Br (Op 311)
	1 Tech Anal & Adv Gr (Op 07T)
	1 Sub Program Br (Op 713)
	1 Tech Support Br (Op 725)
10	CDR, DDC
1	CO & DIR, USNMEL
1	CDR, USNOL
1	DIR, USNRL (Code 2027)
1	CO & DIR, USNUSL
1	CO & DIR, USNEL
1	CDR, USNOTS, China Lake
1	CDR, USNOTS, Pasadena
1	CO, USNUOS
2	NAVSHIPYD PTSMH
2	NAVSHIPYD MARE
1	NAVSHIPYD CHASN
1	SUPSHIP, Groton
1	EB Div, Gen Dyn Corp
1	SUPSHIP, Newport News

Copies	
1	NNSB & DD Co
1	SUPSHIP, Pascagoula
1	Ingalls Shipbldg Corp
1	SUPSHIP, Camden
1	New York Shipbldg
1	DIR DEF, R & E, Attn: Tech Library
1	CO, USNROTC & NAVADMINU, MIT
1	O in C, PGSCOL, Webb
1	DIR, APL, Univ of Washington, Seattle
1	NAS, Attn: Comm on Undersea Warfare
1	Prof. J. Kempner, PIB
1	Dr. E. Wenk, Jr., The White House
1	Dr. R. DeHart, SWRI
1	Mr. Leonard P. Zick, Chicago Bridge & Iron Co.
1	Dean V.L. Salerno, Fairleigh Dickinson Univ.
1	Prof. E.O. Waters, Yale Univ
2	Mr. C.F. Larson, Sec, Welding Research Council
1	Prof. Bernard Budiansky, Harvard Univ
1	Mr. J. Mavor, WHOI

David Taylor Model Basin. Report 1741.
TESTS OF STIFFENED AND UNSTIFFENED MACHINED SPHERICAL SHELLS UNDER EXTERNAL HYDROSTATIC PRESSURE, by Martin A. Krenzke and Thomas J. Kiernan. Aug 1963. iv, 67p. illus., diagrs., graphs, refs.

UNCLASSIFIED

Four series of structural models, consisting of 102 small machined spherical shells, were tested to study the effect of unsupported shell length on both their elastic and inelastic buckling strength. The four series consisted of models representing complete spheres, clamped spherical segment models with included angles ranging from 5 to 300 deg, and stiffened hemispherical models. The collapse pressure of the complete spheres was adequately calculated using the empirical equation earlier developed at the Model Basin. Whereas previous experiments on

1. Spherical shells--Collapse--Model tests
2. Spherical shells (Stiffened)--Collapse--Model tests
3. Spherical shells--Hydrostatic pressure--Model tests
I. Krenzke, Martin A.
II. Kiernan, Thomas J.
III. S-R011 01 01

David Taylor Model Basin. Report 1741.
TESTS OF STIFFENED AND UNSTIFFENED MACHINED SPHERICAL SHELLS UNDER EXTERNAL HYDROSTATIC PRESSURE, by Martin A. Krenzke and Thomas J. Kiernan. Aug 1963. iv, 67p. illus., diagrs., graphs, refs.

UNCLASSIFIED

Four series of structural models, consisting of 102 small machined spherical shells, were tested to study the effect of unsupported shell length on both their elastic and inelastic buckling strength. The four series consisted of models representing complete spheres, clamped spherical segment models with included angles ranging from 5 to 300 deg, and stiffened hemispherical models. The collapse pressure of the complete spheres was adequately calculated using the empirical equation earlier developed at the Model Basin. Whereas previous experiments on

1. Spherical shells--Collapse--Model tests
2. Spherical shells (Stiffened)--Collapse--Model tests
3. Spherical shells--Hydrostatic pressure--Model tests
I. Krenzke, Martin A.
II. Kiernan, Thomas J.
III. S-R011 01 01

David Taylor Model Basin. Report 1741.
TESTS OF STIFFENED AND UNSTIFFENED MACHINED SPHERICAL SHELLS UNDER EXTERNAL HYDROSTATIC PRESSURE, by Martin A. Krenzke and Thomas J. Kiernan. Aug 1963. iv, 67p. illus., diagrs., graphs, refs.

UNCLASSIFIED

Four series of structural models, consisting of 102 small machined spherical shells, were tested to study the effect of unsupported shell length on both their elastic and inelastic buckling strength. The four series consisted of models representing complete spheres, clamped spherical segment models with included angles ranging from 5 to 300 deg, and stiffened hemispherical models. The collapse pressure of the complete spheres was adequately calculated using the empirical equation earlier developed at the Model Basin. Whereas previous experiments on

1. Spherical shells--Collapse--Model tests
2. Spherical shells (Stiffened)--Collapse--Model tests
3. Spherical shells--Hydrostatic pressure--Model tests
I. Krenzke, Martin A.
II. Kiernan, Thomas J.
III. S-R011 01 01

David Taylor Model Basin. Report 1741.
TESTS OF STIFFENED AND UNSTIFFENED MACHINED SPHERICAL SHELLS UNDER EXTERNAL HYDROSTATIC PRESSURE, by Martin A. Krenzke and Thomas J. Kiernan. Aug 1963. iv, 67p. illus., diagrs., graphs, refs.

UNCLASSIFIED

Four series of structural models, consisting of 102 small machined spherical shells, were tested to study the effect of unsupported shell length on both their elastic and inelastic buckling strength. The four series consisted of models representing complete spheres, clamped spherical segment models with included angles ranging from 5 to 300 deg, and stiffened hemispherical models. The collapse pressure of the complete spheres was adequately calculated using the empirical equation earlier developed at the Model Basin. Whereas previous experiments on

1. Spherical shells--Collapse--Model tests
2. Spherical shells (Stiffened)--Collapse--Model tests
3. Spherical shells--Hydrostatic pressure--Model tests
I. Krenzke, Martin A.
II. Kiernan, Thomas J.
III. S-R011 01 01

spherical shells with clamped edges recorded in the literature show a complete lack of repeatability, the results of the present models follow a definite pattern. These tests demonstrate that the unsupported shell length must be relatively short to provide an increase in strength of a spherical segment over that of a complete sphere. They also demonstrate that a small clamped spherical segment may be weaker than a longer clamped segment. The experimental collapse strength of the stiffened shells was in no case as great as would be expected for a machined unstiffened shell of the same weight. Since these were rather exploratory tests, however, they do not demonstrate that effective stiffening systems cannot be developed.

spherical shells with clamped edges recorded in the literature show a complete lack of repeatability, the results of the present models follow a definite pattern. These tests demonstrate that the unsupported shell length must be relatively short to provide an increase in strength of a spherical segment over that of a complete sphere. They also demonstrate that a small clamped spherical segment may be weaker than a longer clamped segment. The experimental collapse strength of the stiffened shells was in no case as great as would be expected for a machined unstiffened shell of the same weight. Since these were rather exploratory tests, however, they do not demonstrate that effective stiffening systems cannot be developed.

spherical shells with clamped edges recorded in the literature show a complete lack of repeatability, the results of the present models follow a definite pattern. These tests demonstrate that the unsupported shell length must be relatively short to provide an increase in strength of a spherical segment over that of a complete sphere. They also demonstrate that a small clamped spherical segment may be weaker than a longer clamped segment. The experimental collapse strength of the stiffened shells was in no case as great as would be expected for a machined unstiffened shell of the same weight. Since these were rather exploratory tests, however, they do not demonstrate that effective stiffening systems cannot be developed.

spherical shells with clamped edges recorded in the literature show a complete lack of repeatability, the results of the present models follow a definite pattern. These tests demonstrate that the unsupported shell length must be relatively short to provide an increase in strength of a spherical segment over that of a complete sphere. They also demonstrate that a small clamped spherical segment may be weaker than a longer clamped segment. The experimental collapse strength of the stiffened shells was in no case as great as would be expected for a machined unstiffened shell of the same weight. Since these were rather exploratory tests, however, they do not demonstrate that effective stiffening systems cannot be developed.